Betzler, C., Eberli, G.P., Alvarez Zarikian, C.A., and the Expedition 359 Scientists
Proceedings of the International Ocean Discovery Program Volume 359
publications.iodp.org

doi:10.14379/iodp.proc.359.108.2017

Site U1470[1]

C. Betzler, G.P. Eberli, C.A. Alvarez Zarikian, M. Alonso-García, O.M. Bialik, C.L. Blättler, J.A. Guo, S. Haffen, S. Horozal, M. Inoue, L. Jovane, D. Kroon, L. Lanci, J.C. Laya, A. Ling Hui Mee, T. Lüdmann, M. Nakakuni, B.N. Nath, K. Niino, L.M. Petruny, S.D. Pratiwi, J.J.G. Reijmer, J. Reolid, A.L. Slagle, C.R. Sloss, X. Su, P.K. Swart, J.D. Wright, Z. Yao, and J.R. Young[2]

Keywords: International Ocean Discovery Program, IODP, *JOIDES Resolution*, Expedition 359, Site U1470, Maldives, Kardiva Channel, Goidhoo atoll, Indian Ocean paleoceanography, Oligocene, Miocene, Pliocene, Pleistocene, carbonate platform, carbonate platform drowning, celestine, dolomite, drift deposits, large benthic foraminifers, monsoon, sea level, sequence stratigraphy

Contents

Background and objectives

Site U1470 (proposed Site MAL-08A) is part of the southern transect of the platform to drift succession cored during Expedition 359. The site (4°45.9823′N, 72°59.0267′E) is located 15.6 km south of Site U1469 at the western entrance of the Kardiva Channel, which connects the open Indian Ocean with the Inner Sea of the Maldives, in a water depth of 399.7 m (Figure **F1**). Inner Sea sediments are

Figure F1. Location map of Site U1470, located in the southern branch of the Kardiva Channel as the eastern site of the southern transect.

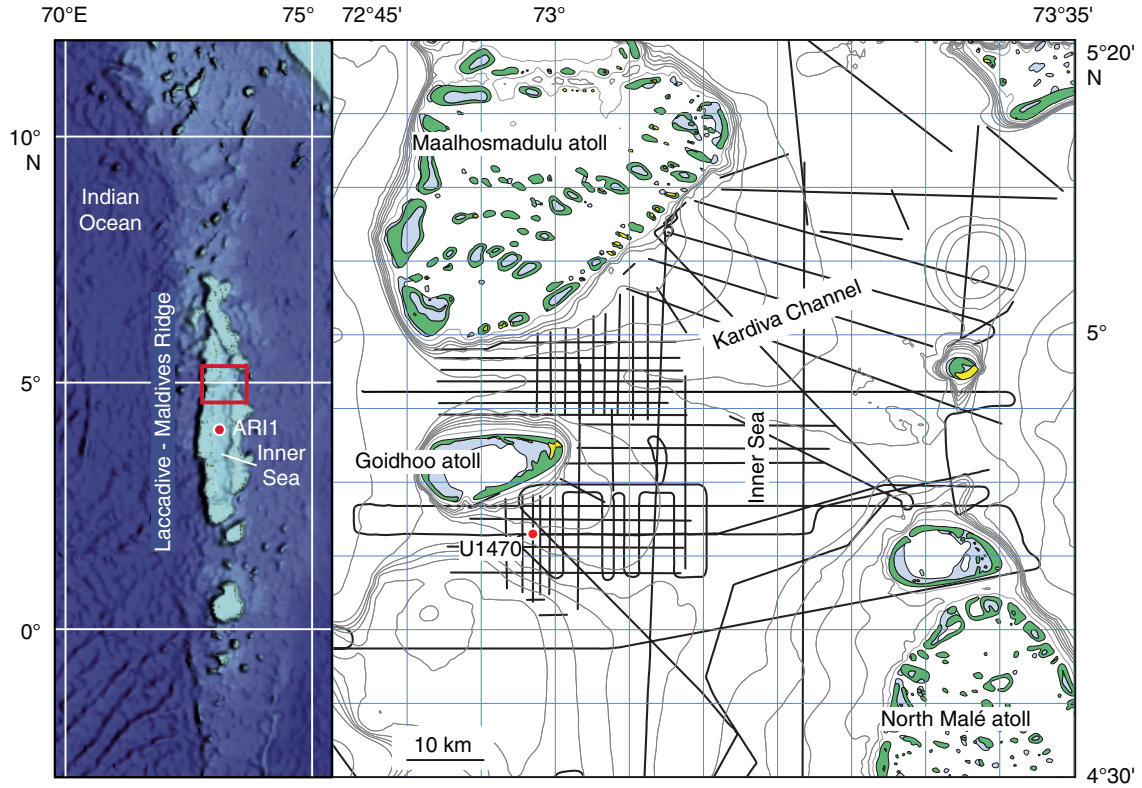

[1] Betzler, C., Eberli, G.P., Alvarez Zarikian, C.A., Alonso-García, M., Bialik, O.M., Blättler, C.L., Guo, J.A., Haffen, S., Horozal, S., Inoue, M., Jovane, L., Kroon, D., Lanci, L., Laya, J.C., Ling Hui Mee, A., Lüdmann, T., Nakakuni, M., Nath, B.N., Niino, K., Petruny, L.M., Pratiwi, S.D., Reijmer, J.J.G., Reolid, J., Slagle, A.L., Sloss, C.R., Su, X., Swart, P.K., Wright, J.D., Yao, Z., and Young, J.R., 2017. Site U1470. *In* Betzler, C., Eberli, G.P., Alvarez Zarikian, C.A., and the Expedition 359 Scientists, *Maldives Monsoon and Sea Level*. Proceedings of the International Ocean Discovery Program, 359: College Station, TX (International Ocean Discovery Program). http://dx.doi.org/10.14379/iodp.proc.359.108.2017

[2] **Expedition 359 Scientists' addresses.**

MS 359-108: Published 4 May 2017

Figure F2. Seismic section along the southern transect with Expedition 359 sites. Site U1470 forms the western end of this southern transect and penetrates through a succession of drift deposits overlying a drowned carbonate bank. Blue horizon = base of drift deposits in the basin. At Site U1470, a stage of carbonate platform growth is observed above this horizon. CDP = common depth point.

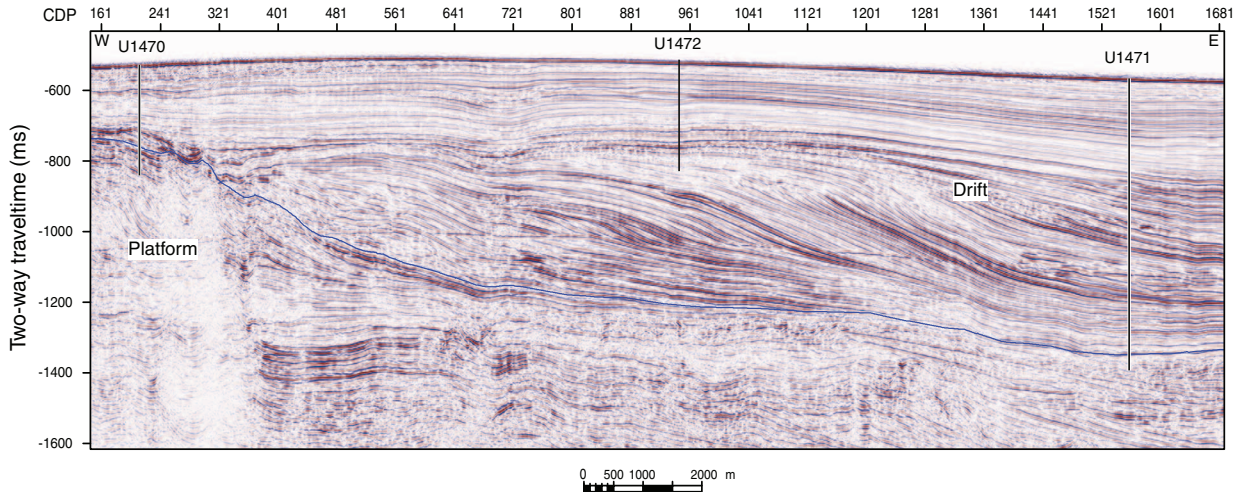

periplatform carbonate oozes consisting of a mixture of components derived from the nearby atolls and pelagic sources. The seafloor is relatively flat and covered by 400 m wide and 4 m high submarine mud waves.

The western termination of the Kardiva Channel is divided into northern and southern branches by the Goidhoo atoll; the southern transect lies in the southern branch. The site was chosen at a position where seismic data indicate that a reef complex evolved above a horizon that correlates with the base of drift sequence (DS) DS1, which defines the platform to drift turnover in the northern transect (Figure **F2**). This seismic relationship implies that at this location platform drowning is younger than in the northern Kardiva Channel.

Site U1470 was chosen to recover the sedimentary succession deposited during the growth of the middle Miocene bank and to characterize the drift sedimentation at this location. Specific objectives were (1) to provide a detailed reconstruction of the predrowning, drowning, and postdrowning evolution of the carbonate bank by linking the seismic stratigraphic record to the sedimentary record (i.e., depositional facies); (2) to constrain the timing of this platform drowning and the burial by drift sediments; and (3) to reconstruct the neritic carbonate factory of a bank growing in the current-dominated depositional system.

Operations

Transit to Site U1470 and Hole U1470A

After a 17.8 nm transit from Site U1469, we arrived at Site U1470 at 2306 h on 14 November 2015. We lowered the thrusters and hydrophones and switched to dynamic positioning mode. We assembled an advanced piston corer (APC)/extended core barrel (XCB) bottom-hole assembly (BHA) and lowered it to the seafloor. After establishing a precision depth recorder depth of 367.0 meters below rig floor (mbrf), the first APC core barrel was deployed, recovering just a water core. The bit was lowered to 403.5 mbrf, and a second APC core barrel was deployed, recovering 2.17 m of core and establishing a seafloor depth of 410.8 mbrf (400.3 meters below sea level [mbsl]). APC coring continued through Core 17H to 148.4 meters below seafloor (mbsf) before a lithologic change in the formation to hard reef material led us to switch to the XCB coring system (see Figure **F1** in the Expedition 359 summary chapter [Betzler et al., 2017b]). Cores 18X and 19X had very poor recovery (0.17 and 0 m, respectively). The material was hard but very friable, and rock pieces broke and jammed in the core catcher. The half-length APC (HLAPC) system was deployed for Cores 20F and 21F, which recovered 1.76 and 1.90 m, respectively. The improved recovery was welcome, but the time required to deepen the hole was a concern. We therefore attempted another XCB core, this time using an "extended" XCB cutting shoe that placed the cutting structure even further ahead of the main drill bit. Recovery with the extended XCB shoe was not better, and because of the higher risk associated with the longer extension of the XCB shoe, it was not run again. Coring was terminated after Core 24X at 190.0 mbsf in favor of starting a new hole using the rotary core barrel (RCB) system. The drill string was pulled clear of the seafloor at 1910 h, and the bit arrived on the rig floor at 2055 h on 15 November, ending Hole U1470A. Total core recovered in Hole U1470A was 139.8 m (74%). Of the 24 cores recovered, 17 were APC cores, 2 were HLAPC cores, and 5 were XCB cores (Table **T1**).

Hole U1470B

By 2400 h on 15 November 2015, we finished making up an RCB BHA and spacing out the core barrels in preparation for lowering the drill string back to the seafloor. The ship was offset 20 m west of Hole U1470A, and Hole U1470B was started at 0230 h on 16 November. An offset seafloor depth of 410.8 mbsl was utilized from adjacent Hole U1470A. Drilling proceeded to 150.0 mbsf before the formation stiffened up enough to warrant deploying a RCB center bit. Drilling continued to 168.9 mbsf, and at 0930 h on 16 November, RCB coring was initiated. Only a single core was cut to 178.6 mbsf before high torque and overpull forced the need for a wiper trip. The drill string was pulled back to 90.2 mbsf, placing the top of the tapered drill collar above seafloor before drilling parameters returned to normal. The hole was washed/reamed to total depth, and at 1345 h on 16 November, RCB coring resumed. Cores 3R–8R to 227.1 mbsf were cut before high torque and overpull indicated cuttings again were not being properly flushed from the hole, perhaps aggravated by zones of lost circulation within the cavernous reefal

Table T1. Site U1470 core summary. DRF = drilling depth below rig floor, DSF = drilling depth below seafloor, CSF = core depth below seafloor. NA = not applicable. H = advanced piston corer, F = half-length advanced piston corer, X = extended core barrel, R = rotary core barrel, numeric core type = drilled interval. (Continued on next page.) **Download table in .csv format.**

Hole U1470A
Latitude: 4°45.9828′N
Longitude: 072°59.0324′N
Water depth (m): 399.7
Date started (UTC): 2230 h; 14 November 2015
Date finished (UTC): 1555 h; 15 November 2015
Time on hole (days):
Seafloor depth DRF (m):
Rig floor to sea level (m): 11.1
Penetration DSF (m): 190
Cored interval (m): 190
Recovered length (m): 139.78
Recovery (%): 73
Drilled interval (m): NA
Drilled interval (no.): 0
Total cores (no.): 24
APC cores (no.): 17
HLAPC cores (no.): 2
XCB cores (no.): 5

Hole U1470B
Latitude: 4°45.9818′N
Longitude: 072°59.0210′N
Water depth (m): 399.72
Date started (UTC): 1555 h; 15 November 2015
Date finished (UTC): 1448 h; 17 November 2015
Time on hole (days): 1.95
Seafloor depth DRF (m): 410.8
Rig floor to sea level (m): 11.08
Penetration DSF (m): 343.7
Cored interval (m): 174.8
Recovered length (m): 7.35
Recovery (%): 4
Drilled interval (m): 168.9
Drilled interval (no.): 1
Total cores (no.): 18
RCB cores (no.): 18

Core	Top of cored interval DSF (m)	Bottom of cored interval DSF (m)	Interval advanced (m)	Recovered length (m)	Curated length (m)	Recovery (%)	Top of recovered core CSF-A (m)	Bottom of recovered core CSF-A (m)	Date (2015)	Time UTC (h)
359-U1470A-										
1H	0.0	2.1	2.1	2.17	2.17	103	0.0	2.17	14 Nov	2245
2H	2.1	11.6	9.5	8.24	8.24	87	2.1	10.34	14 Nov	2325
3H	11.6	21.1	9.5	8.24	8.24	87	11.6	19.84	14 Nov	2355
4H	21.1	30.6	9.5	8.44	8.44	89	21.1	29.54	15 Nov	0030
5H	30.6	40.1	9.5	8.79	8.79	93	30.6	39.39	15 Nov	0100
6H	40.1	49.6	9.5	7.31	7.31	77	40.1	47.41	15 Nov	0125
7H	49.6	59.1	9.5	7.77	7.77	82	49.6	57.37	15 Nov	0150
8H	59.1	68.6	9.5	8.88	8.88	93	59.1	67.98	15 Nov	0210
9H	68.6	78.1	9.5	6.94	6.94	73	68.6	75.54	15 Nov	0240
10H	78.1	87.6	9.5	8.93	8.93	94	78.1	87.03	15 Nov	0300
11H	87.6	97.1	9.5	9.42	9.42	99	87.6	97.02	15 Nov	0325
12H	97.1	106.6	9.5	9.10	9.10	96	97.1	106.20	15 Nov	0415
13H	106.6	116.1	9.5	9.50	9.50	100	106.6	116.10	15 Nov	0440
14H	116.1	125.6	9.5	9.49	9.49	100	116.1	125.59	15 Nov	0505
15H	125.6	135.1	9.5	9.16	9.16	96	125.6	134.76	15 Nov	0540
16H	135.1	144.6	9.5	9.63	9.63	101	135.1	144.73	15 Nov	0625
17H	144.6	148.4	3.8	3.77	3.77	99	144.6	148.37	15 Nov	0645
18X	148.4	158.2	9.8	0.17	0.17	2	148.4	148.57	15 Nov	0810
19X	158.2	163.0	4.8	0.00	0.00	0	158.2	158.20	15 Nov	0840
20F	163.0	165.0	2.0	1.71	1.71	86	163.0	164.71	15 Nov	0925
21F	165.0	167.0	2.0	1.90	1.90	95	165.0	166.90	15 Nov	0950
22X	167.0	172.0	5.0	0.07	0.07	1	167.0	167.07	15 Nov	1100
23X	172.0	180.3	8.3	0.00	0.00	0	172.0	172.00	15 Nov	1155
24X	180.3	190.0	9.7	0.15	0.15	2	180.3	180.45	15 Nov	1245
	Hole U1470A totals:		190.0	139.78	139.78					
359-U1470B-										
11	0.0	168.9		*****Drilled from 0.0 to 168.9 mbsf*****					16 Nov	0355
2R	168.9	178.6	9.7	0.24	0.24	2	168.9	169.14	16 Nov	0435
3R	178.6	188.3	9.7	0.13	0.13	1	178.6	178.73	16 Nov	0925
4R	188.3	198.0	9.7	0.13	0.13	1	188.3	188.43	16 Nov	0950
5R	198.0	207.7	9.7	3.46	3.46	36	198.0	201.46	16 Nov	1040
6R	207.7	217.4	9.7	0.98	0.98	10	207.7	208.68	16 Nov	1125
7R	217.4	227.1	9.7	0.60	0.60	6	217.4	218.00	16 Nov	1220
8R	227.1	236.8	9.7	0.06	0.06	1	227.1	227.16	16 Nov	1555
9R	236.8	246.5	9.7	0.00	0.00	0	236.8	236.80	16 Nov	1635
10R	246.5	256.2	9.7	0.13	0.13	1	246.5	246.63	16 Nov	1655
11R	256.2	265.9	9.7	0.00	0.00	0	256.2	256.20	16 Nov	1720
12R	265.9	275.6	9.7	0.06	0.06	1	265.9	265.96	16 Nov	1755
13R	275.6	285.4	9.8	0.29	0.29	3	275.6	275.89	16 Nov	1830
14R	285.4	295.1	9.7	0.07	0.07	1	285.4	285.47	16 Nov	1920
15R	295.1	304.8	9.7	0.10	0.10	1	295.1	295.20	16 Nov	2000
16R	304.8	314.5	9.7	0.07	0.07	1	304.8	304.87	16 Nov	2040
17R	314.5	324.3	9.8	0.20	0.20	2	314.5	314.70	16 Nov	2125

Table T1 (continued).

Core	Top of cored interval DSF (m)	Bottom of cored interval DSF (m)	Interval advanced (m)	Recovered length (m)	Curated length (m)	Recovery (%)	Top of recovered core CSF-A (m)	Bottom of recovered core CSF-A (m)	Date (2015)	Time UTC (h)
18R	324.3	334.0	9.7	0.72	0.72	7	324.3	325.02	16 Nov	2205
19R	334.0	343.7	9.7	0.11	0.11	1	334.0	334.11	16 Nov	2255
	Hole U1470B totals:		343.7	7.35	7.35					

limestone. Another 3 h wiper trip was made, and at 2030 h, RCB coring restarted. Coring continued through Core 19R to 343.7 mbsf, and coring was terminated shortly after 0400 h to wireline log the hole. Downhole logging was considered to be of greater importance than deepening a challenging hole. The shifting tool was run in the hole; however, there were problems shifting the mechanical bit release sleeve to release the bit. Repeatedly jarring on the sleeve with the wireline jars eventually knocked the sleeve loose, and the bit was released at 0530 h. The sleeve was reverse shifted without incident, and the drill string was pulled to logging depth at 100.2 mbsf.

Because of the uncertainty about hole conditions and stability, a single logging run was planned with a tool string designed to measure the highest priority data (gamma ray, sonic velocity, electrical resistivity, and borehole diameter). Rig-up for wireline logging began at 0730 h on 17 November. We ran this sonic-resistivity tool string into the hole without installing the nuclear source, but unfortunately, resistance was encountered almost immediately as the tools reached 10 m below the end of the pipe, and we were not able to securely pass a collapsing section of the borehole just 52 m below the end of the pipe at 100.2 mbsf. The winch operator eventually pulled the tool string back into the pipe and up to the rig floor, where it was rigged down, and logging operations in Hole U1470B were concluded by 1215 h on 17 November. The drill string was pulled clear of the seafloor at 1230 h, and the drill string was recovered back onboard ship with the end of the pipe clearing the rig floor rotary table at 1355 h. The positioning beacon was recovered on deck at 1410 h. Thrusters were pulled, and the rig was secured for transit to the next site. Total core recovered in Hole U1470B was 7.35 m (4%). Eighteen RCB cores were recovered (Table **T1**).

Lithostratigraphy

Site U1470 is located on the southern transect of Expedition 359 in a setting similar to that of Sites U1465 and U1469 on the northern transect. A succession of hemipelagic deposits and shallow marine deposits of the Kardiva platform was recovered from Site U1470. The Kardiva platform is an isolated aggrading to prograding carbonate platform that partly drowned in the middle Miocene (Belopolsky and Droxler, 2004; Betzler et al., 2013a; Lüdmann et al., 2013). Five lithostratigraphic units were identified at Site U1470 based on visual core descriptions and smear slide and thin section analyses from cores collected in Holes U1470A and U1470B (Figure **F3**):

Unit I: unlithified planktonic foraminifer–rich grainstone to packstone.
Unit II: partly lithified bioclastic packstone to grainstone.
Unit III: dolomitic coral-rich rudstone and floatstone.
Unit IV: large benthic foraminifer–rich rudstone and grainstone.
Unit V: coral-rich floatstone to packstone.

Figure F3. Lithostratigraphic summary, Site U1470.

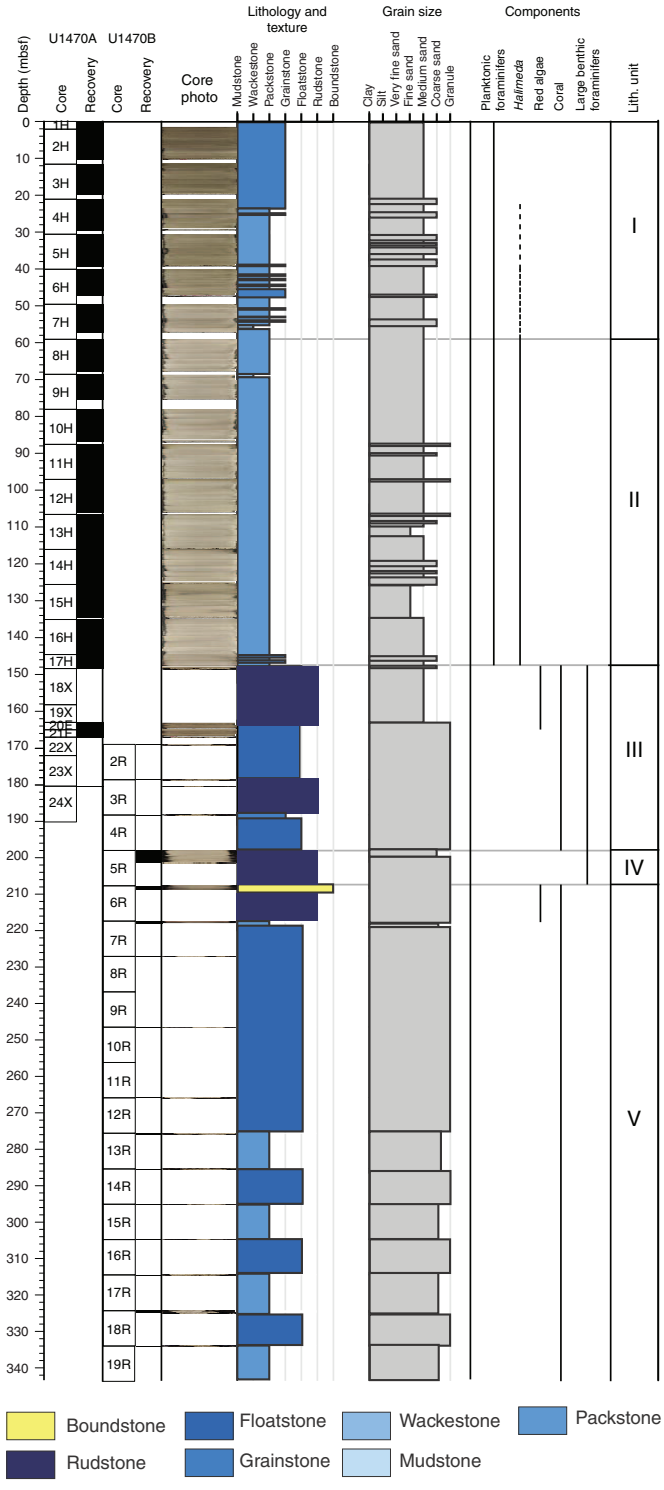

Lithostratigraphic units

Unit I

Interval: 359-U1470A-1H-1, 0 cm, to 7H-CC, 13 cm
Depth: 0–59.1 mbsf

Unit I consists of unlithified gray-brown to pale yellow medium- to coarse-grained grainstone to packstone. Planktonic foraminifers are the dominant skeletal grains (Figure **F4A**), with common benthic foraminifers, pteropods, echinoderm spines, bryozoan fragments, and bivalves. Yellow-red–stained lithic grains are common. Rare bryozoan and red algae fragments are also present. Occasionally, apatite is present in the unit (Figure **F4B**).

Unit II

Interval: 359-U1470A-8H-1, 0 cm, to 17H-3, 28 cm
Depth: 59.1–148.1 mbsf

The transition from Unit I to Unit II at 59.1 mbsf is marked by a change to (1) a lighter color identified in the visual core descriptions and supported by lightness (L*) values (Figure **F5**) and (2) a considerable change to poorer preservation of skeletal grains. Unit II is a pale yellow medium- to coarse-grained partially lithified planktonic foraminifer-rich grainstone to packstone. Bivalve fragments, benthic foraminifers, and echinoderm spines are common in this unit, as well as abundant unidentified skeletal grains. Bryozoan fragments are also present. Skeletal grains are poorly preserved and difficult to identify because of the overgrowth of calcite cements.

The sharp contact between Units II and III was identified at 17H-3, 50 cm (148.1 mbsf). The sharp boundary is represented by a

Figure F4. Smear slide images from Unit I. A. Planktonic foraminifers (1) are the main skeletal component (359-U1470A-4H-2, 125 cm). B. Apatite (2) is present in a few intervals.

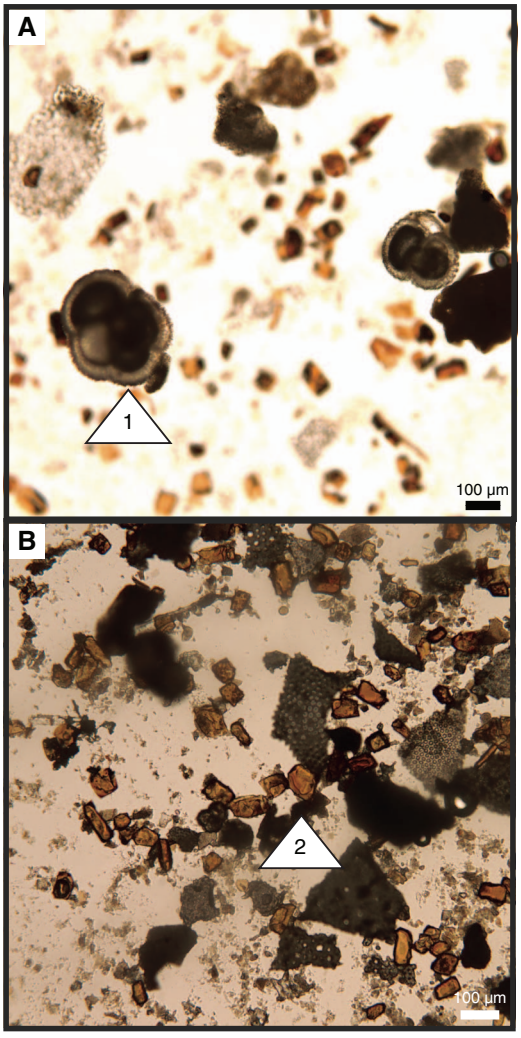

Figure F5. Transition from Unit I (359-U1470A-7H-CC) to Unit II (8H-1). Visually distinct color change to lighter tones in photos corresponds with shift to higher L*.

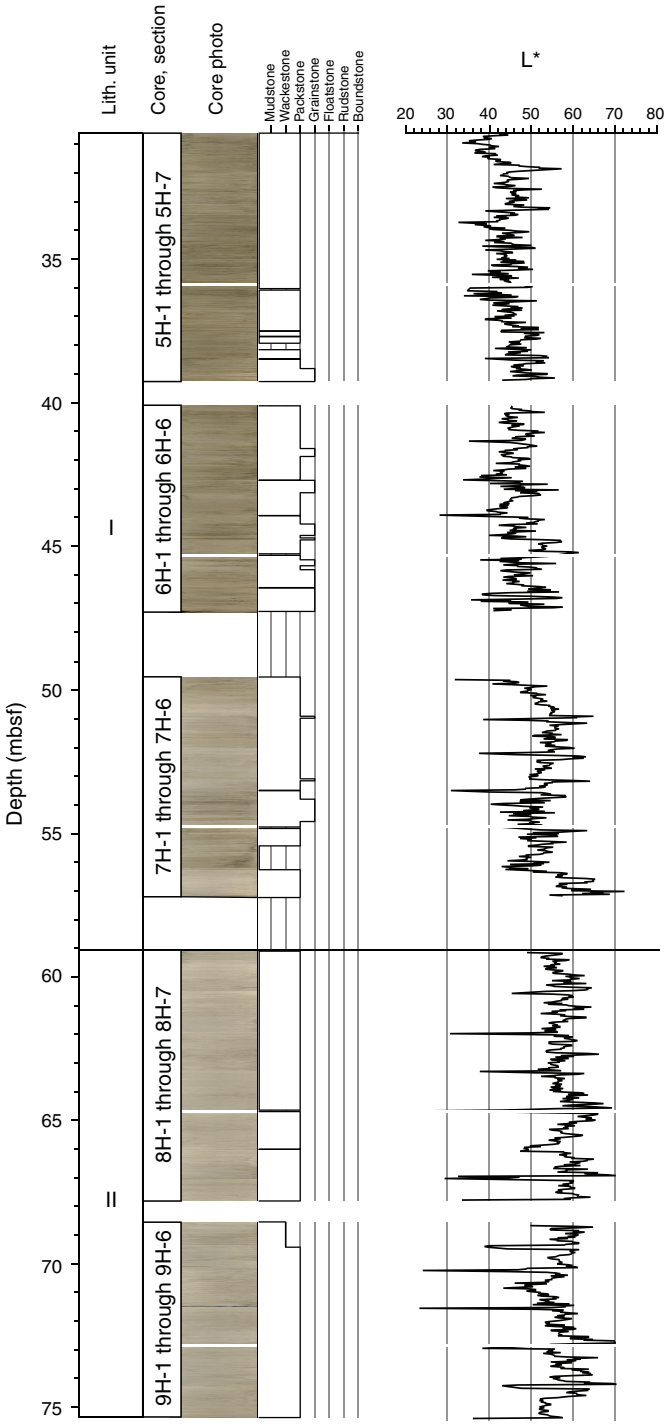

Figure F6. Unit II/III boundary (359-U1470A-17H-3) at 148.10 mbsf with change from packstone–grainstone to dolomitized floatstone–rudstone with corals.

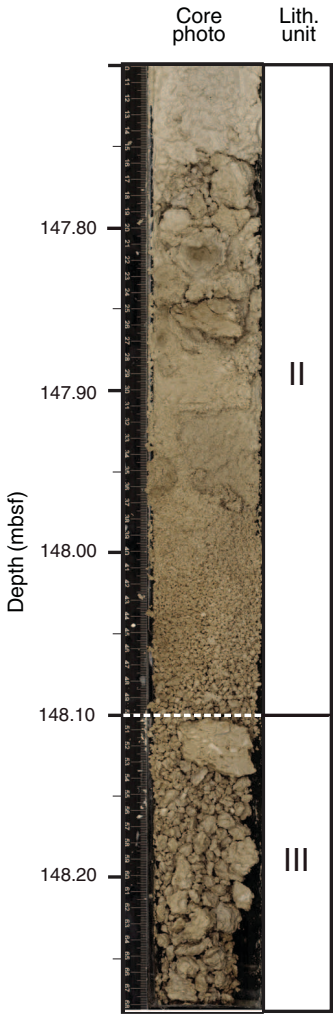

distinct color change from white to pale brown and a lithologic change from medium- to coarse-grained packstone–grainstone to dolomitized floatstone–rudstone with corals, mollusks, bivalves, and large benthic foraminifers (Figure F6).

Unit III

Intervals: 359-U1470A-17H-3, 28 cm, to 24X-CC, 21 cm; 359-U1470B-2R-CC, 0 cm, to 4R-CC, 13 cm
Depth: 148.1–198 mbsf

Unit III consists of grayish brown coarse- to granule-grained slightly dolomitic coral-rich floatstone to rudstone. The main components include abundant coral fragments (massive, platy, and branching), encrusting red algae, and encrusting foraminifers (Figure F7). Molds of bivalves and gastropods are common to abundant. Irregular nodule-shaped rhodoliths, up to 2 cm in diameter, are present. Some borings were observed that indicate bioerosion of a consolidated substrate. Large red algae bioclasts are abundant, but large benthic foraminifers (*Amphistegina* sp.), bryozoan, and mollusk fragments are also common. Dolomite cements and bladed, dogtooth, and drusy calcite are present, as well as poikilotopic cements with crystals ~50 µm. Most components are dissolved and occur as large molds.

Figure F7. Main components, Unit III. A. Massive coral fragment (359-U1470B-2R-CC, 15–19 cm). B. Branching red algae (2R-CC, 19–22 cm).

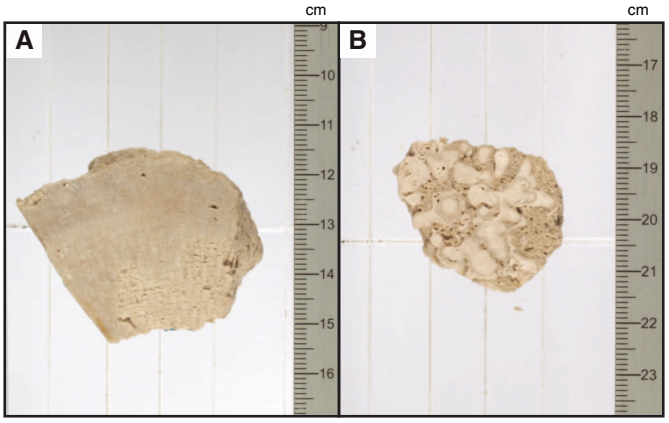

Figure F8. Large benthic foraminiferal grainstone characteristic of Unit IV (359-U1470B-5R-2, 15–25 cm). 1 = shell fragment, 2 = large benthic foraminifer (*Lepidocyclina* sp.).

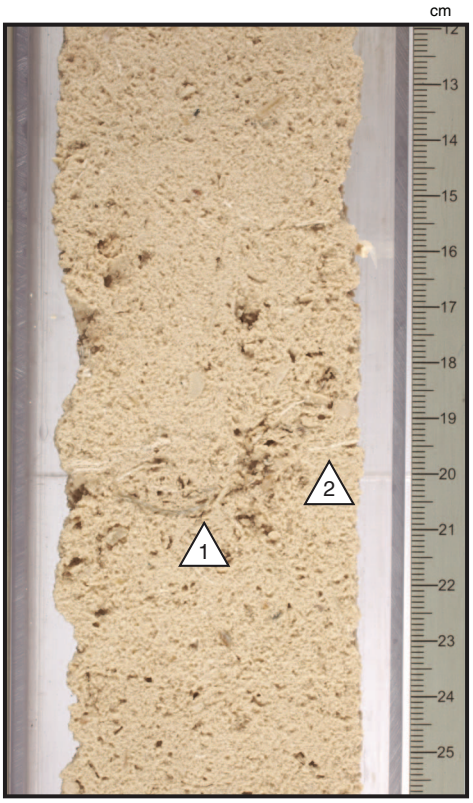

Unit IV

Interval: 359-U1470B-5R-1, 0 cm, to 5R-CC, 17 cm
Depth: 198–207.4 mbsf

Unit IV is a succession of pale yellow medium- to coarse-grained bioclastic-rich grainstone to rudstone. Bioclastic grains are abundant, and large benthic foraminifers (*Lepidocyclina* sp.) are the main recognizable skeletal grains (Figure F8). Red algae and green algae (*Halimeda*) are present. Coral fragments were identified, but only very few coarse clasts are present. The components present are red algae, large benthic foraminifers (*Amphistegina* sp.), mollusk

Figure F9. Bioclastic rudstone, Unit IV (359-U1470B-5R-3, 23–26 cm; plane-polarized light). 1 = *Lepidocyclina* sp., 2 = *Amphistegina* sp., 3 = partially dissolved *Halimeda* fragment, 4 = echinoderm fragment.

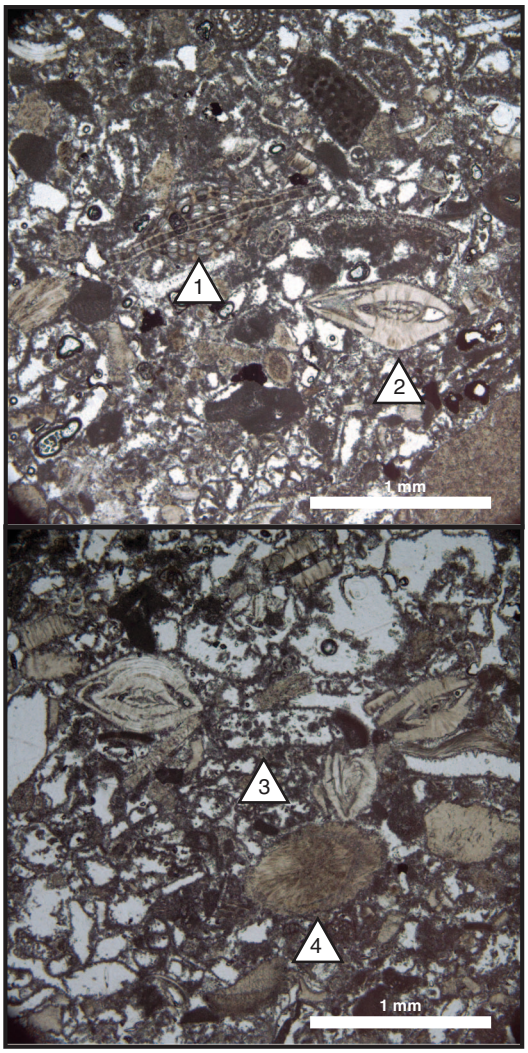

fragments, and echinoid fragments (Figure **F9**). Most components are dissolved into molds, whereas undissolved components are micritized. Bladed, dogtooth, and drusy calcite cements are present, as well as poikilotopic cements with crystals up to 250 µm. Bladed calcite is usually observed around pore walls and infilling pore spaces.

Unit V

Interval: 359-U1470B-6R-1, 0 cm, to 19-CC, 11 cm
Depth: 207.4–334.11 mbsf

Unit V consists of dolomitized coarse- to granule-grained grayish brown coral-rich floatstone to boundstone and red algae with a very poorly sorted matrix. The main components include abundant coral fragments (massive, platy, and branching), encrusting red algae, encrusting foraminifers, small and large benthic foraminifers (*Amphistegina* and miliolids), mollusk fragments, bryozoans, red algae, coral fragments, and *Halimeda* as skeletal grains (Figure **F9**). Large mollusk shells (2–6 cm long) are significant features in the unit. Molds of bivalves and gastropods are common to abundant (Figure **F10**). Rhodoliths, up to 4 cm wide with branching irregular

Figure F10. Floatstone, Hole U1470B. A. Red algal floatstone (6R-1, 30–37 cm). 1 = gastropod mold, 2 = rhodolith, 3 = mollusk mold. B. Coral-rich floatstone (7R-1, 27–57 cm). 4 = branching coral, 5 = large mollusk shell.

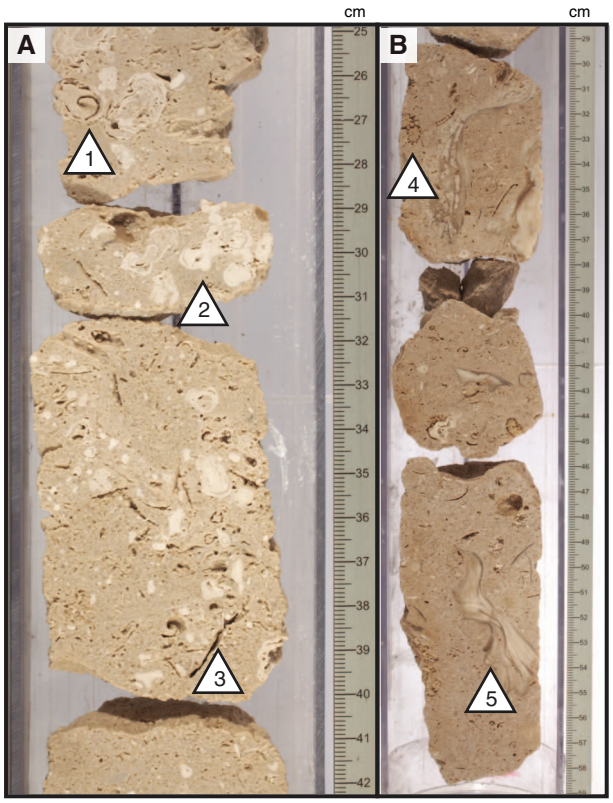

shapes, are present. Geopetal infill within a complete bivalve shell was observed. Fine crystals of dolomite are also present and are responsible for the very pale brown color of the unit. Most components are dissolved into molds or micritized. Calcite cements include drusy, fibrous, poikilotopic, and syntaxial overgrowths with crystal sizes up to 700 µm.

Discussion

The lithology of Unit I consists of coarse-grained and very well sorted bioclastic grainstone to packstone. The deposits are associated with a moderate- to high-energy current regime that dominated the Kardiva Channel during the Pliocene–Pleistocene. The bioclasts present are typical open-marine pelagic fauna with a minor proportion of skeletal benthic fauna that may be derived from the active shallow-marine carbonate factory and transported by currents to the Inner Sea.

In addition to the color change to lighter color, one of the main arguments to separate Unit II from Unit I is the beginning of poor preservation of skeletal grains. In the poorly sorted interbedded packstone and wackestone intervals, open pelagic fauna (e.g., planktonic foraminifers) is mixed with neritic fauna (e.g., large benthic foraminifers and mollusks). This alternation of texture and mixing of bioclasts is likely the result from fluctuations in current intensity.

The Unit II/III boundary is a hardground on top of the platform carbonates; however, the surface is not as clear as the one at Site U1469 because drilling did not recover the transition precisely. Hardground surfaces such as those identified at Sites U1469 and U1470 represent a break in sedimentation due to a change of depositional environment and a cessation in carbonate production. The

Figure F11. Increase in crystal size from Unit III to Unit V. A. Syntaxial overgrowth of echinoderm fragment (359-U1470B-5R-3, 23–26 cm). B. Poikilotopic cement (18R-1W, 16–18 cm).

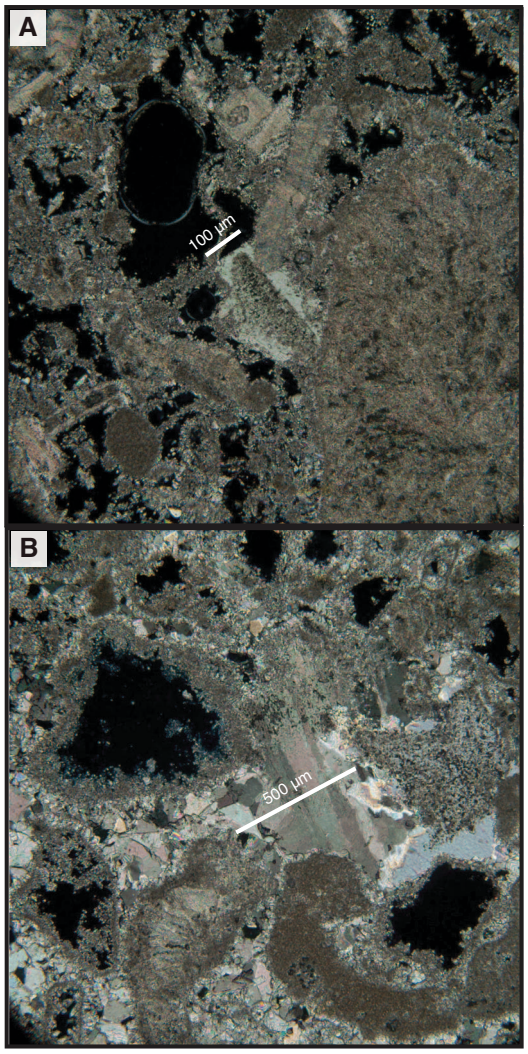

change in depositional environment is related to the drowning of the carbonate factory (e.g., Betzler et al., 2009).

Unit III sediments are marked by fragments of massive and branching corals, rhodoliths, gastropods, and other encrusting organisms that were deposited in a shallow-marine reef to fore-reef environment. The fragmented and well-preserved character of the reefal material recovered indicates an origin in sand patches present within the reef framework structure. Unit IV is interpreted as a shallow-marine subtidal intrareef setting influenced by currents as evidenced by clean reworked bioclastic grainstone to rudstone (Riegl et al., 2007).

The sedimentary characteristics of Unit V indicate deposition in a shallow-marine reef to back-reef setting as evidenced by the occurrence of massive, platy, and branching coral; red algae; mollusks; and encrusting organisms. The branching and platy corals are probably still in living position and represent water depths of 0–35 or 0–15 m, depending on the water transparency (Hallock, 2005). The large mollusks, red algae encrustations, and other bioclastic material represent skeletal sands deposited in a back-reef setting, similar to the present-day back-reef to lagoonal deposits of the Bahamas (Ginsburg, 1958). A slight change in water depth can be inferred for the period in which only red algae and platy coral developed, as platy corals represent water depth conditions between 10–15 and 20–35 m (Hallock, 2005). This interval is overlain by facies dominated by branching coral and large benthic foraminifers and most likely reflects a shallower environment located closer to the reef crest.

In summary, the five lithostratigraphic units represent two depositional environments that dominate the sedimentation processes: (1) a current-driven depositional system that includes Units I and II, in which pelagic-dominated sediments are deposited, and (2) a shallow-marine environment dominated by reef-building organisms. The latter includes carbonate platform Units III–V that cover reef to intrareef and back-reef facies realms. Calcite cementation gradually increases from Unit III to Unit V. Crystal size increases from ~50 to 700 µm, perhaps because of a constant solute supply through pore water advection or dissolution of skeletal grains and a slightly longer residence time (Harris et al., 1985) (Figure **F11**). In addition, dolomite is present in Units III–V. Sedimentation patterns observed at the Marion Plateau show a fairly similar platform development and demise history (Ehrenberg et al., 2006; Eberli et al., 2010), as well as associated dolomitization patterns. Ehrenberg et al. (2006) propose that dolomitization at the Marion Plateau resulted from circulation of normal to slightly modified seawater. Swart (2000) reported on similar dolomitization patterns in Great Bahama Bank.

Biostratigraphy

A ~334 m sequence was recovered from Site U1470. The uppermost ~147 m consists of calcareous drift sediments; the remainder to the bottom of the borehole consists of well-cemented limestones. Calcareous plankton is present throughout the drift sequence. In the upper part (from the top to Core 359-U1470A-7H) preservation and abundance are adequate to allow a biostratigraphy to be reasonably well established for the site. In the lower part, only sparse long-ranging nannofossils are present and planktonic foraminifers are poorly preserved. Nonetheless, planktonic foraminifers allowed a tentative age model for this part of the sequence. Planktonic foraminiferal stratigraphy suggests a late Miocene age for the interval just above the drowned platform.

Age model

The sequence of recognized biostratigraphic events is summarized in Table **T2**. The biozonation inferred from those events and the paleoenvironmental interpretations are plotted in Figure **F12**. The age-depth plot and derived average sedimentation rates are displayed in Figure **F13**. In the upper part of the sequence, through the Quaternary and early Pliocene, a useful sequence of biostratigraphic events was found; however, as at other sites, planktonic foraminifers consistently indicate older ages and therefore lower sedimentation rates than calcareous nannofossils. A compromise regression line based on both groups gives an average sedimentation rate of ~2.2 cm/ky.

For the lower part of the core, through the early Pliocene and possibly the latest Miocene, only a single planktonic foraminiferal event was identified. This finding suggests that the average sedimentation rate remained constant throughout the Pliocene at ~2.2 cm/ky and that the base of the drift sequence is older than 5.92 Ma.

Table T2. Biostratigraphic events, Site U1470. FO = first occurrence, LO = last occurrence. Occurrence of *S. abies* is sporadic until Sample 359-U1470A-11H-CC, 97 cm, so LO maybe lower than indicated here. N = nannofossil, PF = planktonic foraminifer. Ages are based on Gradstein et al. (2012). See Raffi et al. (2006) for a review of nannofossil events and original sources for correlations to magnetostratigraphic timescales. **Download table in .csv format.**

Event	Abbreviation	Fossil group	Age (Ma)	Age reference	Core, section, interval (cm) last sample above event	Core, section, interval (cm) first sample below event	Top depth (mbsf)	Bottom depth (mbsf)	Midpoint depth (mbsf)
					359-U1470A-	359-U1470A-			
FO *Emiliania huxleyi*	F *E.h*	N	0.29	Hilgen et al. (2012)	1H-CC	2H-CC	2.17	10.34	6.3
LO *Pseudoemiliania lacunosa*	L *P.l*	N	0.44	Hilgen et al. (2012)	1H-CC	2H-CC	2.17	10.34	6.3
Start small *Gephyrocapsa* event	S *sG*	N	1.24	Hilgen et al. (2012)	3H-CC	4H-CC	19.84	29.54	24.7
LO *Discoaster brouweri*	L *D.b*	N	1.93	Hilgen et al. (2012)	5H-CC	6H-CC	39.39	47.41	43.4
LO *Discoaster pentradiatus*	L *D.p*	N	2.39	Hilgen et al. (2012)	6H-CC	7H-2, 103	47.41	52.02	49.7
LO *Sphenolithus abies*	L *S.a*	N	3.54	Hilgen et al. (2012)	7H-CC	11H-CC	57.32	97.02	77.2
LO *Globigerinoides ruber* pink	L *G.rp*	PF	0.12	Thompson et al. (1979)	1H-1, mudline	1H-CC	0.00	2.17	1.1
LO *Globigerinoides fistulosus*	L *G.f*	PF	1.88	Lourens et al. (2004)	4H-CC	5H-CC	29.54	39.39	34.5
LO *Globorotalia limbata*	L *G.l*	PF	2.39	Lourens et al. (2004)	5H-CC	6H-CC	39.39	47.41	43.4
LO *Dentoglobigerina altispira*	L *D.a*	PF	3.47	Lourens et al. (2004)	6H-CC	7H-3, 35–36	47.41	52.57	50.0
LO *Globoquadrina dehiscens*	L *G.d*	PF	5.92	Wade et al. (2011)	13H-CC	16H-CC	116.10	144.60	130.4

Figure F12. Biostratigraphic and paleoenvironmental summary, Site U1470. Calcareous nannofossil and planktonic foraminifer biozonation is shown with paleoenvironmental information provided by benthic foraminifers and ostracods.

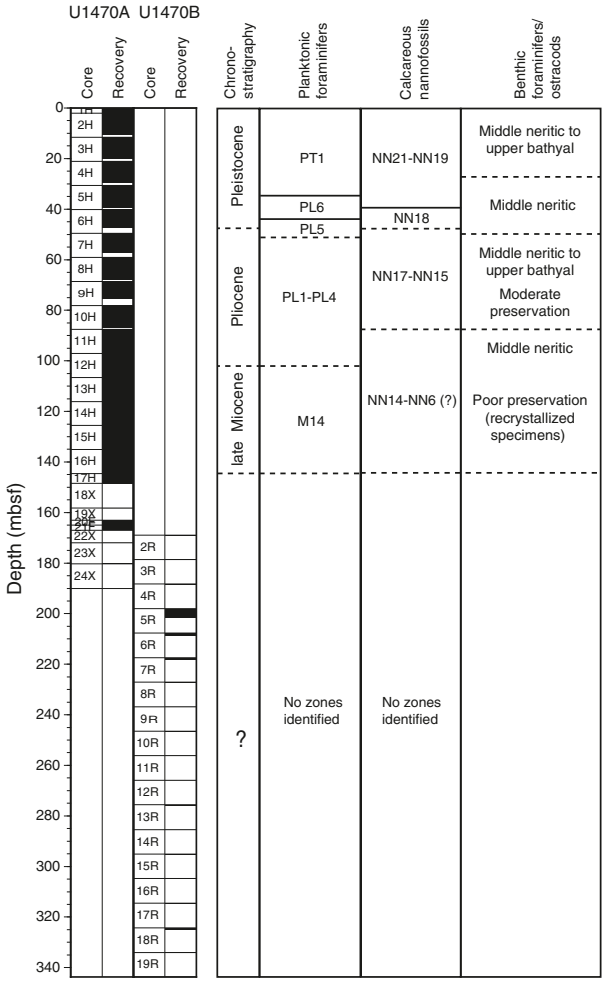

Calcareous nannofossils

Nannofossils were examined from all core catcher samples in the drift sequence (Cores 359-U1470A-1H through 17H) and from several additional samples from the lower part of the sequence (Table T3). Nannofossils are abundant and well preserved in the uppermost core catcher sample, but preservation and abundance deteriorate downhole.

A tentative age model was suggested for the upper part of the sequence (Cores 1H–7H). *Emiliania huxleyi* is present in Sample 1H-CC but absent from Sample 2H-CC (both confirmed by scanning electron microscope examination) and *Pseudoemiliania lacunosa* is absent from Sample 1H-CC but present in Sample 2H-CC. Therefore, the first occurrence (FO) of *E. huxleyi* (0.29 Ma) and the last occurrence (LO) of *P. lacunosa* (0.44 Ma) can both be placed in

Figure F13. Age-depth plot, Site U1470. Details of each event plotted are given in Table T2.

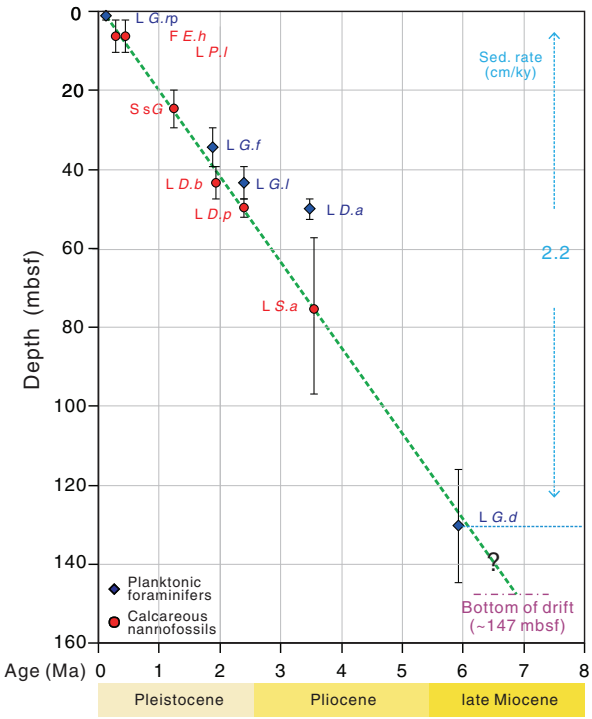

Table T3. Nannofossil range chart, Hole U1470A. **Download table in .csv format.**

the interval between the two samples, and it is not possible to differentiate Zones NN19–NN21. The assemblage in Sample 3H-CC is dominated by diverse small *Gephyrocapsa* specimens (<3 µm long). The assemblages in Sample 4H-CC are similar, with the addition of medium to large *Gephyrocapsa lumina*. The base of the small *Gephyrocapsa* event (1.24 Ma) was placed between these samples. *Discoaster brouweri* was first observed in Sample 6H-CC, and *Discoaster pentaradiatus* was first observed in Sample 7H-2, 103 cm.

Below Core 7H, the diversity and abundance of nannofossils decrease drastically, and no events can be confidently placed. *Sphenolithus abies* is present in the lower part of the core, but it is rare and sporadic in Samples 8H-CC to 10H-CC, so it is not clear where its FO takes place. No discoasters or ceratoliths were observed in this part of the sequence, so it is not possible to determine whether the Miocene was reached.

Planktonic foraminifers

Planktonic foraminifers were examined in Hole U1470A core catcher samples (16 samples) until the drilling reached the drowned carbonate platform (Core 17H). One additional sample was taken from Section 7H-3. Planktonic foraminifers show good preservation from the top to Sample 7H-CC, where foraminifers start to show calcite overgrowth, but they are present in all samples.

Three Pleistocene bioevents were identified in Hole U1470A: the LO of *Globigerinoides ruber* pink (0.12 Ma) between the mudline sample and Sample 1H-CC (~1.1 mbsf), the LO of *Globigerinoides fistulosus* (1.88 Ma) between Samples 4H-CC and 5H-CC (~34.5 mbsf), and the LO of *Globorotalia limbata* (2.39 Ma) between Samples 5H-CC and 6H-CC (~43.4 mbsf). Within the Pliocene, we identified the LO of *Dentoglobigerina altispira* (3.47 Ma) between Samples 6H-CC and 7H-3W, 35–36 cm (~50 mbsf), and the LO of *Globoquadrina dehiscens* (5.92 Ma) between Samples 13H-CC and 16H-CC (~130.4 mbsf) (Tables **T2**, **T4**). Constraints on this event are limited because only a few specimens of *G. dehiscens* were identified and because Samples 15H-CC, 14H-CC, and 13H-CC show poor preservation and very low abundances of planktonic foraminifers. Nonetheless, we were able to make a tentative estimate of the age of the sediments just above the drowned platform. The presence of *G. dehiscens* (LO = 5.92 Ma) and *Neogloboquadrina acostaensis* in Section 16H-CC (139.7 mbsf; above the drowned platform) suggests a late Miocene age for this part of the sequence.

Benthic foraminifers

Seventeen core catcher samples and one core section sample (359-U1470A-7H-3W, 35–36 cm) from Hole U1470A were investigated for benthic foraminifers. Samples from the top of the sequence contain abundant Pleistocene benthic foraminifers that range from very good to good preservation (Table **T5**). Specimens of benthic foraminifers from this interval include *Cancris* sp., *Discanomalina* sp., *Neorotalia calcar*, and *Planulina ariminensis*, indicating a middle neritic to upper bathyal depositional environment.

In Samples 4H-CC through 6H-CC, preservation changes to moderate. Bolivinids (smooth and flat) increase slightly in abundance during this interval as well. Below Sample 7H-3W, 35–36 cm, preservation decreases sharply downhole, and all benthic foraminifers picked in this interval show calcite overgrowth (Figure **F12**). Therefore, most specimens were identified to the genus level only. Samples from the late Miocene and Pliocene intervals all show poor preservation with low abundance and diversity of benthic foraminifers. Specimens from these intervals are dominated by *Amphistegina* sp., *Reusella* sp., and *Stilostomella* sp. Above the drowned platform at the base of this sequence, bolivinids become increasingly abundant again in Sample 16H-CC. No large benthic foraminifers were recovered from the platform interval in the core catcher samples studied. Throughout Hole U1470A, echinoderm spine fragments are abundant. Fish teeth (unidentified species) are present in several samples from the Pleistocene section and rare in several samples from the late Miocene to Pliocene intervals.

Table T4. Planktonic foraminifer range chart, Hole U1470A. **Download table in .csv format.**

Table T5. Benthic foraminifer range chart, Hole U1470A. **Download table in .csv format.**

Table T6. Ostracod range chart, Hole U1470A. **Download table in .csv format.**

Ostracods

Samples 359-U1470A-1H-CC to 16H-CC and 7H-3W, 35–36 cm, were examined for ostracods, which are present in all samples as single valves and complete carapaces. They are most abundant in the upper half of the sequence, which corresponds to the Pliocene–Pleistocene. The observed reduction in abundance may be related to preservation, which varies from good and moderate in Samples 1H-CC to 7H-3W, 35–36 cm, to poor in Samples 7H-CC to 16H-CC. Poorly preserved specimens are heavily overgrown, and some are fragmented.

Ostracods were identified preliminarily to the genus level (Table **T6**). Compared to Sites U1465–U1468, the overall ostracod assemblage is remarkably uniform through time, predominantly composed of Bairdiids, with *Loxoconcha*, *Mutilus*, *Bradleya*, *Caudites*, and *Microxestoleberis* as secondary taxa. Bairdiids are found from neritic to bathyal depths, but an increase in their relative abundance and diversity is typically associated with shallow-water marine environments (Warne, 1998). Inner to middle neritic conditions are also indicated by the presence of *Loxoconcha*, *Caudites*, *Mutilus*, and *Leptocythere*. In contrast, the common occurrence of *Bradleya* in Samples 1H-CC to 3H-CC, 7H-3W, 35–36 cm, and 7H-CC suggest an increase in water depth to upper bathyal conditions from Middle to Late Pleistocene and in the late Pliocene, respectively (Figure **F12**). *Cytheropteron*, a common bathyal genus (Zhao et al., 2000), is also present in Sample 1H-CC.

Radiolarians

Six core catcher samples from Hole U1470A were prepared for radiolarian analysis. Radiolarians were almost barren in the core catcher samples analyzed at this site.

Geochemistry

Interstitial water chemistry

Interstitial water (IW) sampling from Hole U1470A was limited by poor recovery, with only 16 samples obtained from whole-round squeezing. Lithification and poor recovery prevented IW sampling below ~150 mbsf. No IW samples were obtained from Hole U1470B. Concentrations of all measured species are given in Table **T7**.

Major ions and salinity

Major anion and cation concentrations generally remain constant and close to the mean seawater value throughout the sampled interval. The Cl^- concentrations measured using titration with $AgNO_3$ vary between 564 and 568 mM (Figure **F14**). Concentrations of SO_4^{2-} also remain stable throughout Hole U1470A (~29 mM).

The concentration of Na^+ ranges between 477 and 485 mM. The concentration of K^+ remains stable throughout the sampled interval at approximately 10 mM. Similarly stable values are reflected in Ca^{2+} and Mg^{2+}, which range between 10.9 and 11.6 mM and 53.1 and 56.2 mM, respectively (Figure **F15**). Salinity remains relatively constant at 34.5–35 throughout the measured interval. No trends are present in major ions and salinity with increasing depth.

Minor ions, alkalinity, and pH

Analysis of minor ions by inductively coupled plasma–atomic emission spectroscopy (ICP-AES) shows no significant trends with depth for Sr^{2+}, Li^+, Fe, Ba^{2+}, $B(OH)_4^-$, or Si (Figure **F15**; Table **T7**). Alkalinity values mostly range from 2.5 to 3.1 mM, slightly higher than the mean seawater value (Figure **F16**). The pH decreases from 7.91 at the surface to 7.65 at 17 mbsf and remains stable at approximately 7.6 below this depth.

Table T7. Interstitial water chemistry, Site U1470. **Download table in .csv format.**

Figure F14. IW Cl^-, Na^+, K^+, and SO_4^{2-} concentrations, Hole U1470A.

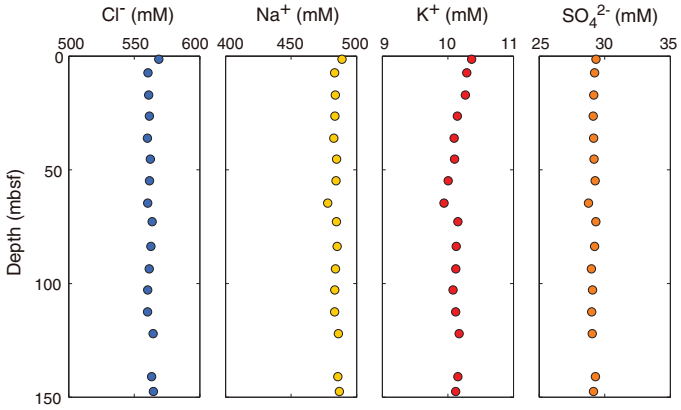

Figure F15. IW Ca^{2+}, Mg^{2+}, and Sr^{2+} concentrations, Hole U1470A.

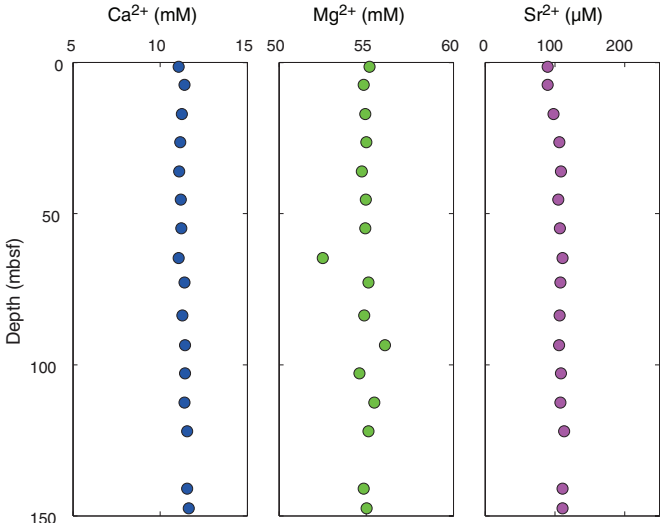

Bulk sediment geochemistry

Calcium carbonate and organic matter

Calcium carbonate content was determined at a rate of one per section for 68 samples. Carbonate content ranges between 80 and 100 wt% with the majority of the data falling between 90 and 98 wt% (Figure **F17**; Table **T8**).

Total organic carbon concentrations were measured on one sample per core in Holes U1470A and U1470B and are generally less than 0.5 wt% with four high values (~1 to ~4 wt%) at 2.7, 12.3, 78.8, and 208.5 mbsf. Total nitrogen is less than 0.1 wt%.

X-ray diffraction

Mineralogy was determined at a rate of approximately one sample per core. In the upper 148 mbsf, the sediment consists of between 25% and 62% aragonite, with the remainder composed of low-Mg calcite (LMC) and small amounts of high-Mg calcite (HMC) and dolomite (Figure **F18**; Table **T9**). HMC is only present near the surface (upper 8 mbsf). Aragonite suddenly disappears below 148 mbsf, and LMC becomes predominant with a dolomite peak at 180 mbsf (32.3%) and small amounts of aragonite between

Figure F16. IW alkalinity and hydrogen (pH) concentrations, Hole U1470A.

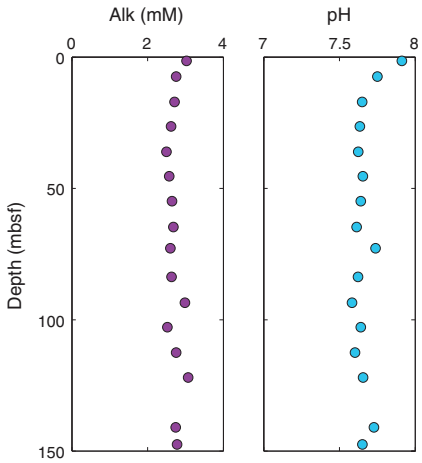

Figure F17. Carbonate and organic carbon contents, Site U1470.

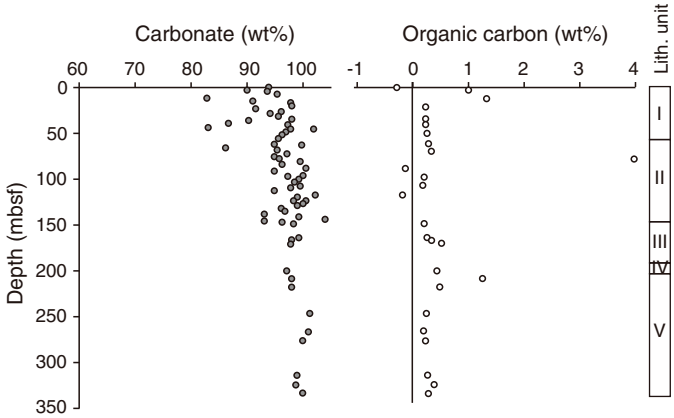

Table T8. Carbon and nitrogen, Site U1470. **Download table in .csv format.**

Figure F18. Relative concentrations of aragonite, HMC, LMC, dolomite, and quartz measured using XRD, Site U1470.

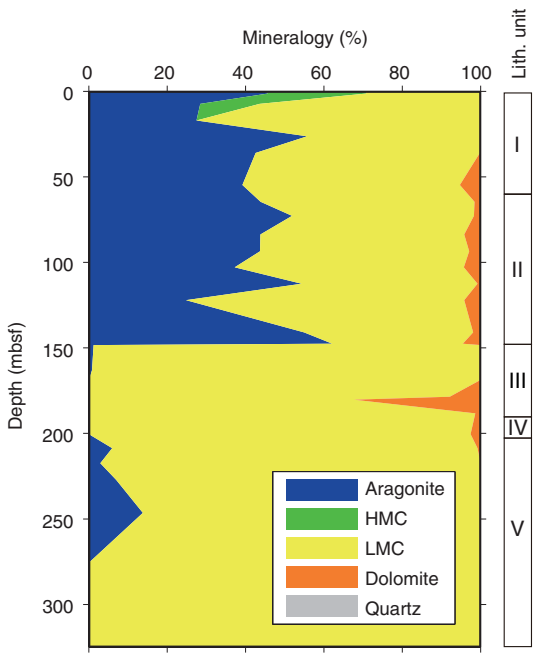

Table T9. XRD results, Site U1470. **Download table in .csv format.**

209 and 247 mbsf. Quartz concentrations are less than 0.2% throughout Holes U1470A and U1470B.

Major, minor, and trace element composition

Minor and trace element concentrations were measured on the same sediment samples measured for X-ray diffraction (XRD) and on two other samples (359-U1470A-6H-4, 0 cm, and 359-U1470B-19R-CC). The most important elements relevant to carbonate diagenesis (Sr, Mg, Fe, and Mn) are presented in Figure **F19** as molar ratios relative to calcium. All data are presented in Table **T10**.

Strontium and magnesium

The Mg/Ca ratios are variable, ranging from 0.3 to 3.1 mmol/mol, and decrease overall from 2.7 mmol/mol at the surface to 0.8 mmol/mol at the bottom of Hole U1470B. In addition, a peak corresponds to an occurrence of dolomite at 180 mbsf (Figure **F18**). The range of Sr/Ca ratios at Site U1470 is similar to that observed at Site U1466 (~4 mmol/mol). The Sr/Ca in bulk sediments varies between 0.4 and 3.5 mmol/mol and changes abruptly at 150 mbsf, corresponding to the change from aragonite- to LMC-dominant mineralogy (Figure **F18**). Within the upper 150 mbsf, the average Sr/Ca ratio is 2.50 mmol/mol, whereas below this depth the average is 0.59 mmol/mol.

Manganese and iron

The Mn/Ca ratios are higher in the upper 50 mbsf, averaging 64.5 µmol/mol, and then decrease to ~38 µmol/mol and remain stable from 50 to 150 mbsf. The 16 mmol/mol decrease in Mn/Ca occurs at 150 mbsf, becoming relatively stable again (~25 mmol/mol) below that depth to the bottom of Hole U1470B (Figure **F19**). Ratios of Fe/Ca are similar to the trend found in Mn/Ca with an average value of 122.5 µmol/mol in the upper 50 mbsf. Below this depth, Fe/Ca is relatively stable at around 40 µmol/mol. Both Mn/Ca and Fe/Ca have small peaks at 180 mbsf that correspond to the small dolomite peak.

Figure F19. Mg/Ca, Sr/Ca, Mn/Ca, and Fe/Ca ratios in sediments, Site U1470.

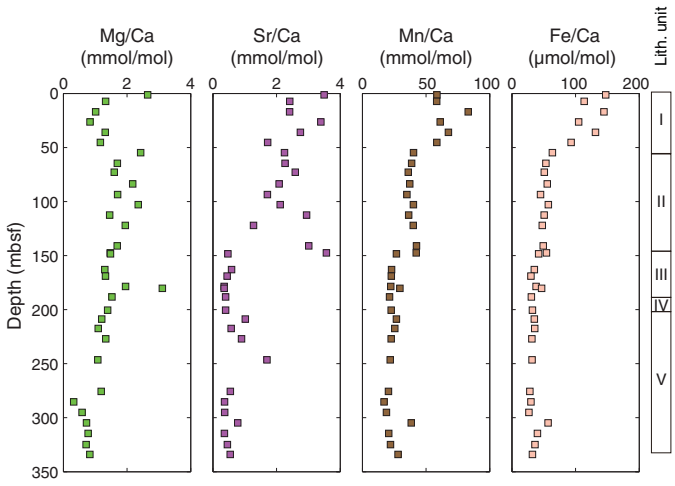

Table T10. Solids geochemistry, Site U1470. **Download table in .csv format.**

Figure F20. Headspace methane concentrations, Site U1470.

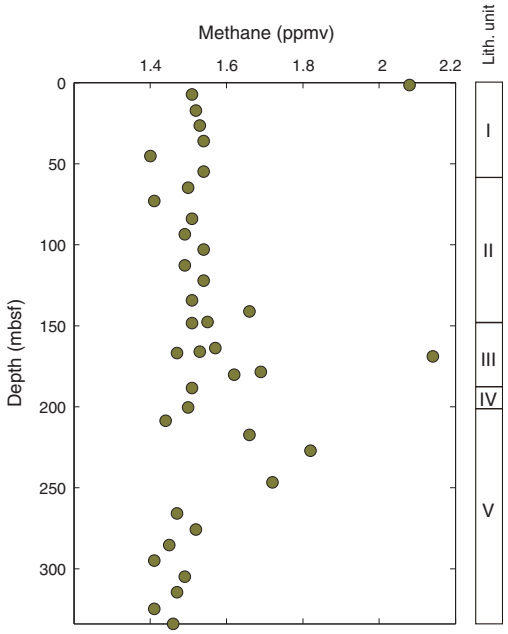

Table T11. Headspace hydrocarbons, Site U1470. **Download table in .csv format.**

Volatile hydrocarbons

Headspace samples for the analysis of methane, ethene, ethane, propene, and propane were taken from every core at Site U1470. These samples were generally taken from the top of Section 5 in each Hole U1470A core when an IW sample was taken. In Hole U1470B, headspace samples were generally taken from Section 1 or core catcher sediments. Methane remains mainly less than 2 ppmv throughout Site U1470 with a small peak around 230 mbsf (Figure **F20**; Table **T11**).

Discussion

Interstitial water chemistry

In contrast to Sites U1466–U1468, where changes in IW chemistry were observed, no definitive trends occur in any of the chemical species measured at Site U1470 (Figures **F14**, **F15**, **F16**). Major and minor ion concentrations are essentially identical to mean seawater values, and this trend is similar to the one found at Site U1465. As at Site U1465, this general lack of variation could result from high-permeability sediments that allow rapid advection. Otherwise, there might be negligible rates of modern diagenesis at this location, similar to those at Site U1465.

The excess (or deficit) of SO_4^{2-}, alkalinity, Ca^{2+}, and Mg^{2+} relative to Cl^- is calculated using Equation **1** to unravel changes in these parameters as a result of changes in salinity (Figure **F21**):

$$\text{Excess sulfate (mM)} = SO_4^{2-}{}_{\text{sample}} - SO_4^{2-}{}_{\text{seawater}} \times [Cl^-{}_{\text{sample}}/Cl^-{}_{\text{seawater}}]. \quad (1)$$

Unlike Site U1468, there are no significant variations. Although a slight increase in excess Ca^{2+} is found below 60 mbsf, this trend appears to be negligible compared to that found at Site U1468 (~5 mmol).

Carbonate diagenesis

The mineralogical changes shown by the XRD data reflect carbonate diagenesis during sediment burial. Aragonite and HMC are metastable and readily undergo neomorphism to LMC. The relatively high concentration of aragonite between 26% and 62% throughout the late Miocene to Pleistocene (0–150 mbsf) reflects variations in input rather than diagenetic change to LMC (Figure **F18**). The disappearance of aragonite at 150 mbsf is coincident with the lithostratigraphic Unit II/III boundary and might suggest a period of exposure to meteoric fluids. Variations in Sr/Ca ratios reflect variations in the percentage of aragonite in the upper portion of the core (~150 mbsf) (Figures **F18**, **F19**). This sudden decrease is also found in Mn/Ca and Fe/Ca ratios, although the decreasing ranges are smaller than that of Sr/Ca ratios. On the other hand, Mg/Ca ratios do not reflect the changes in aragonite concentrations, but the Mg/Ca peak at 180 mbsf clearly reflects the presence of dolomite. In addition, small peaks of Mn/Ca and Fe/Ca ratios at 180 mbsf are probably related to dolomitization.

Changes in Mn/Ca and Fe/Ca ratios might reflect variations in redox chemistry and incorporation of the reduced forms (Mn^{2+} and Fe^{2+}) of these elements into diagenetic carbonates as seen in sediment samples from Site U1466 (Figure **F19**). Although no variations are found in Mn and Fe in IW samples (Figure **F15**; Table **T7**), higher sedimentary Mn/Ca and Fe/Ca ratios from the surface to 50 mbsf, coincident with Unit I, reflect moderately reduced conditions.

Figure F21. Excess SO_4^{2-}, Mg^{2+}, Ca^{2+}, and alkalinity, Site U1470.

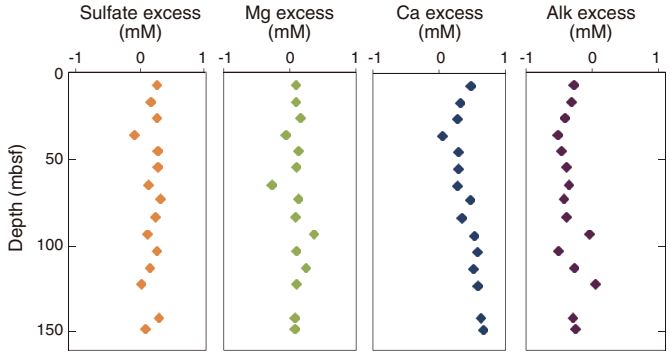

Paleomagnetism

The natural remanent magnetization (NRM) from 17 APC and 2 HLAPC cores from Hole U1470A were routinely measured at 10 cm intervals using the superconducting rock magnetometer (SRM) and subjected to stepwise alternating field (AF) demagnetization at 15 and 30 mT. Results are summarized in Figure **F22**.

Figure F22. NRM intensity, declination, and inclination of APC cores, Hole U1470A. As at other sites, the upper part of each core shows extremely large NRM intensities, which were interpreted as drill pipe contamination. Below 60 mbsf (Core 8H), an obvious artifact in the declination and inclination record assumes a constant direction of ~090°/00°.

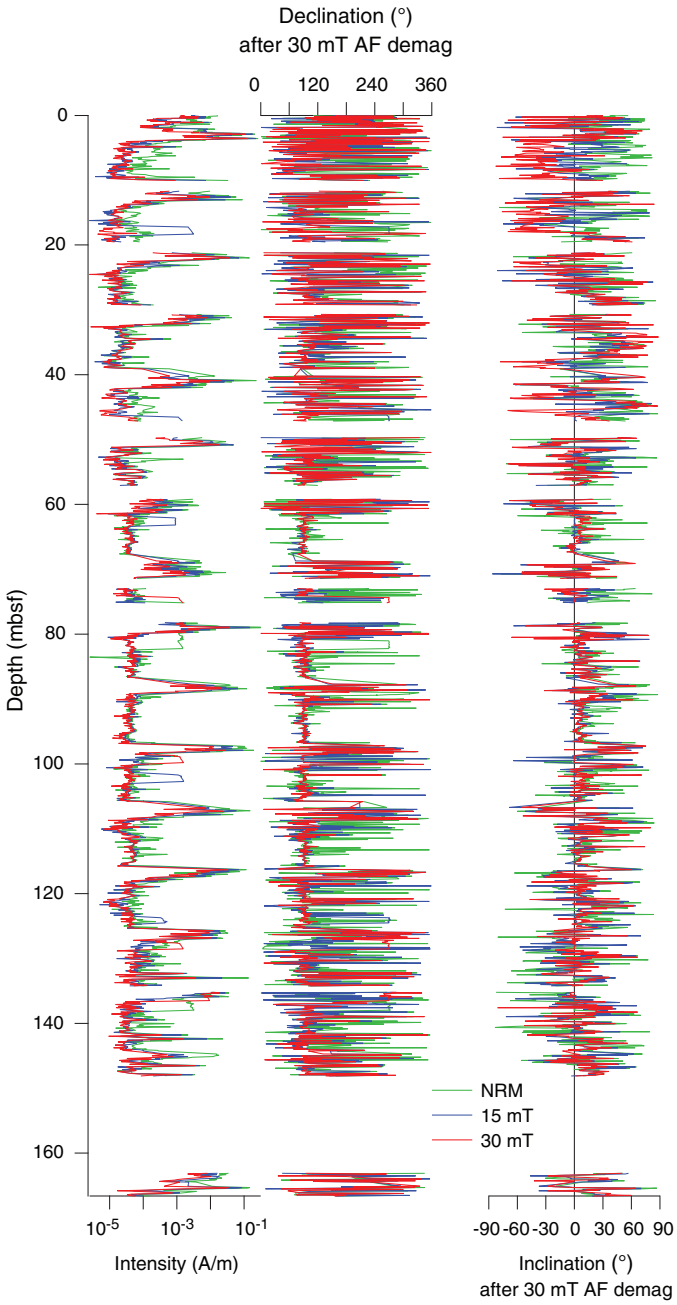

Figure F23. Magnetic moment, Hole U1470A. A. *X*, *Y*, and *Z* components after demagnetization at 30 mT and removal of highly magnetized intervals with magnetization >1 × 10^{-4} A/m. *Y* component shows two distinct distributions below and above 60 mbsf. We assume the difference is due to a bias in the measurements that was tentatively corrected by subtracting a moment of 2 × 10^{-9} A/m² to all cores below 60 mbsf. B. Corrected *Y* component of measurements taken below 60 mbsf compared with original *X*, *Y*, and *Z* components.

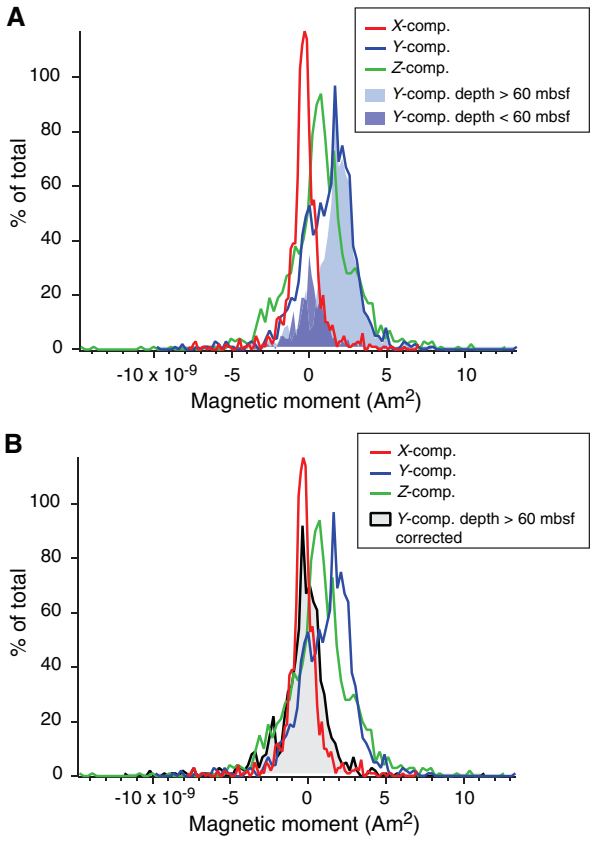

In addition to the persistent contamination affecting the uppermost two sections of every core that was recognized at Site U1467, Hole U1470A data showed a novel artifact that mostly affected measurements below 60 mbsf. Starting from Core 8H, the measured paleomagnetic directions of the "uncontaminated" portion of each core (i.e., the part with remanent magnetization intensity <1 × 10^{-4} A/m) showed a constant direction toward east with a subhorizontal inclination (~090°/00°) independent from the actual core orientation. This suggests that the *Y*-axis superconducting quantum interference device (SQUID) sensor was biased toward high values. Although the cause of this artifact is not understood, the bias in the *Y*-axis component is clearly shown in Figure **F23**, which compares the distribution of magnetic moments of the *X*, *Y*, and *Z* components. The magnitude of the bias was estimated by comparing the mode of the sets of measurements below and above 60 mbsf, which was valued at about 2 × 10^{-9} A/m². We tentatively attempted to correct this artifact by subtracting 2 × 10^{-9} A/m² from the *Y* component of cores from below 60 mbsf (i.e., Core 8H through Section 17H-3) to remove their bias compared to cores from above 60 mbsf (i.e., Cores 1H–7H). The inclinations and declinations resulting from this correction are shown in Figure **F24**. Although not necessarily valid, the corrected directions look reasonably credible, suggesting the presence of some reversals in the declination record.

Figure F24. NRM intensity, declination, and inclination of APC cores following removal of high-intensity peaks, Hole U1470A. Green lines = possible geomagnetic reversals as shown by changes in declination within a single core.

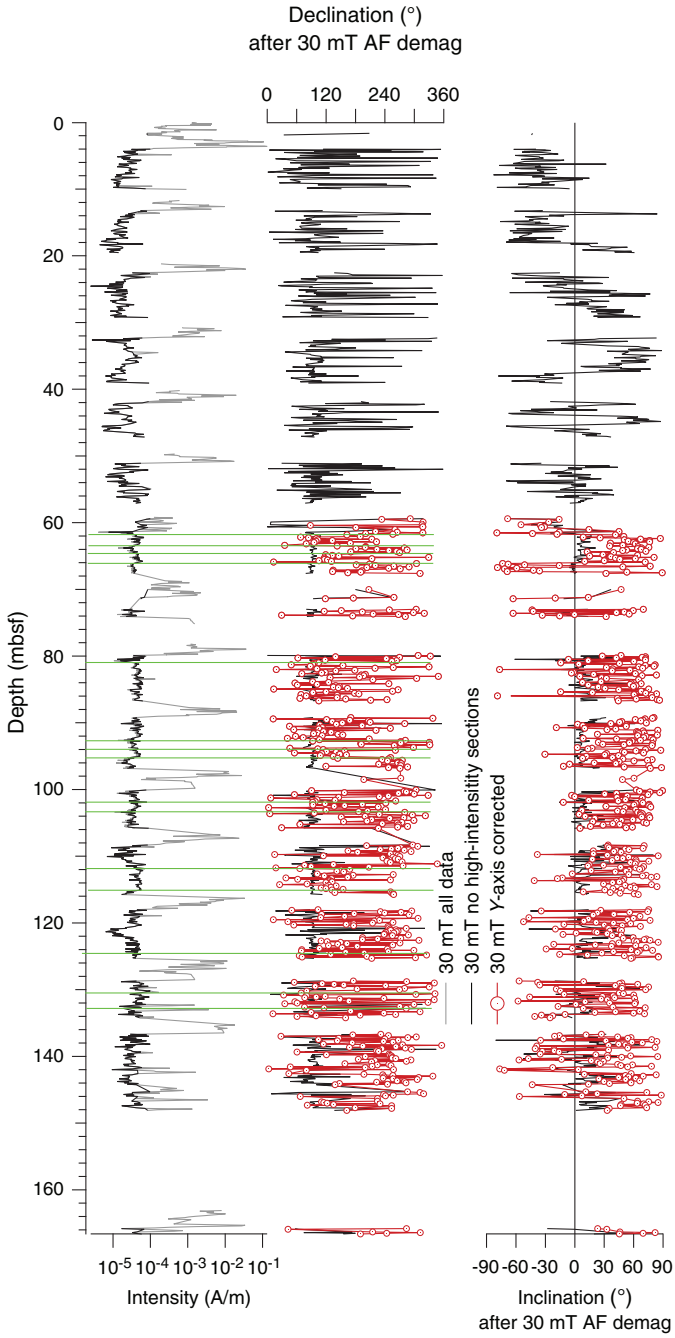

Paleomagnetic results

Possible reversals deduced from the changes in declination are marked with green lines in Figure **F24**. However, inclination has

rather high values, and given all the uncertainties associated with these measurements, we did not attempt to interpret these results as a record of geomagnetic polarity changes.

Physical properties

Density, porosity, natural gamma radiation (NGR), color reflectance, magnetic susceptibility (MS), *P*-wave velocity, thermal conductivity, and shear strength measurements were performed on Cores 359-U1470A-1H through 21F and 359-U1470B-5R through 18R (Figures **F25**, **F26**, **F27**). Thermal conductivity was measured only on soft sediments recovered from the upper 166 mbsf, whereas sediment shear strength was only measured on the interval from 55 to 115 mbsf. *P*-wave velocity was measured using the *P*-wave caliper (PWC) on discrete cylinder samples and pieces from split cores without liners. Density and porosity measurements were performed on moisture and density (MAD) samples obtained once every other section from both soft sediments and hard rocks.

The sedimentary succession from the two holes is divided into three petrophysical (PP) units based on changes in NGR, *P*-wave velocity, bulk density, and porosity. These units can be partially correlated to thermal conductivity and color reflectance L* (Figures **F26**, **F27**). Unit 1 extends to 54 mbsf and comprises the Pleistocene drift sediments, which are the upper part of the Pliocene–Pleistocene drift identified by Betzler et al. (2013b) and Lüdmann et al. (2013). Unit 2 (54–148 mbsf) is likely the late Miocene portion of the drift (see **Biostratigraphy**) and is petrophysically recognized by low NGR that rapidly increases downhole accompanied by increasing bulk density and a concomitant decrease in porosity; all other properties display little change. Unit 3 (148–334.1 mbsf) within the carbonate platform succession is identified by the abrupt increase of velocity and density. Porosity decreases below ~170 mbsf. Thermal

Figure F25. Color reflectance (L*, a*, and b*) and magnetic susceptibility measured with MSL and MSP, Site U1470.

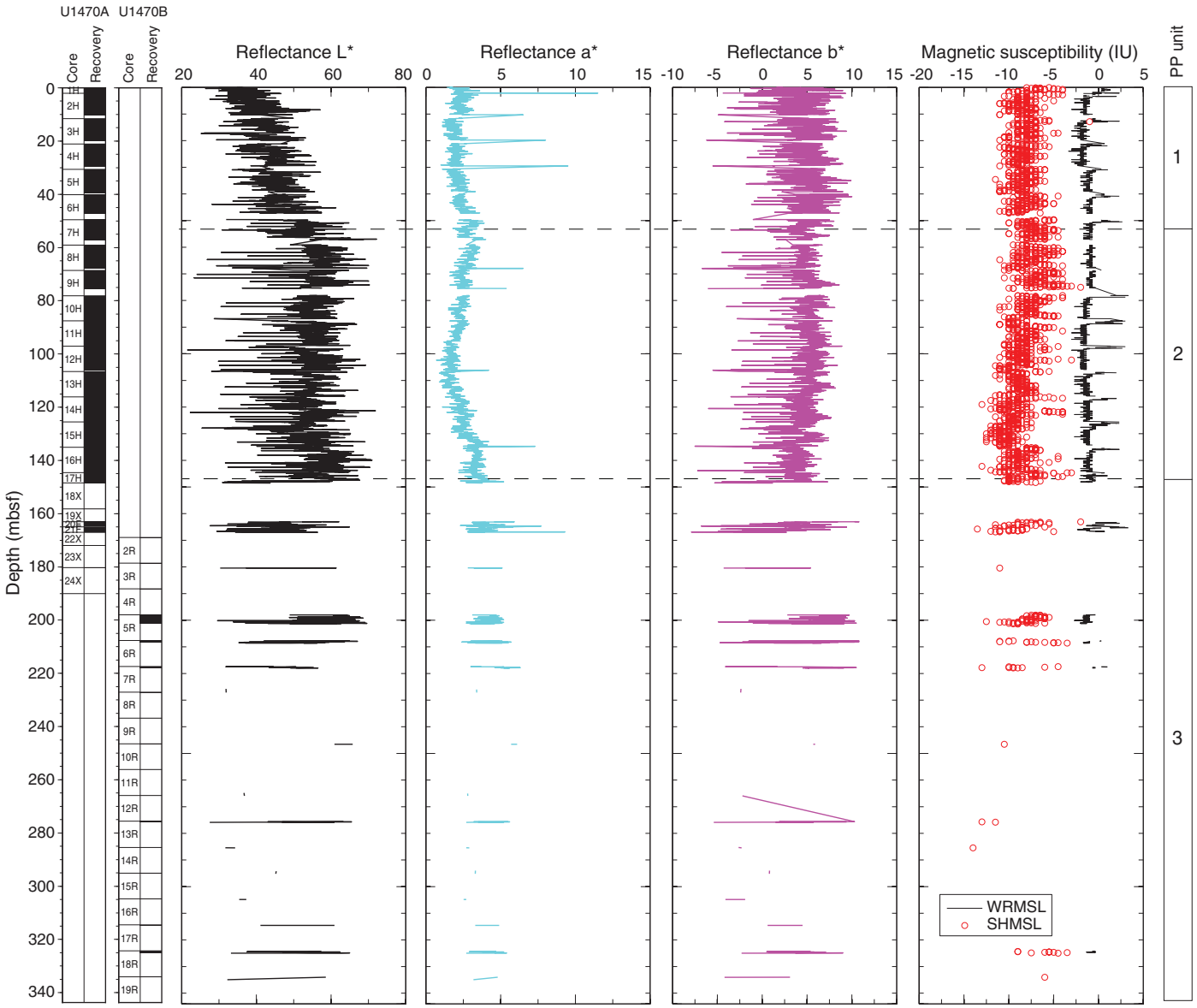

Figure F26. NGR, GRA and MAD bulk density, grain and dry density, porosity, and *P*-wave velocity on WRMSL and PWC, Site U1470.

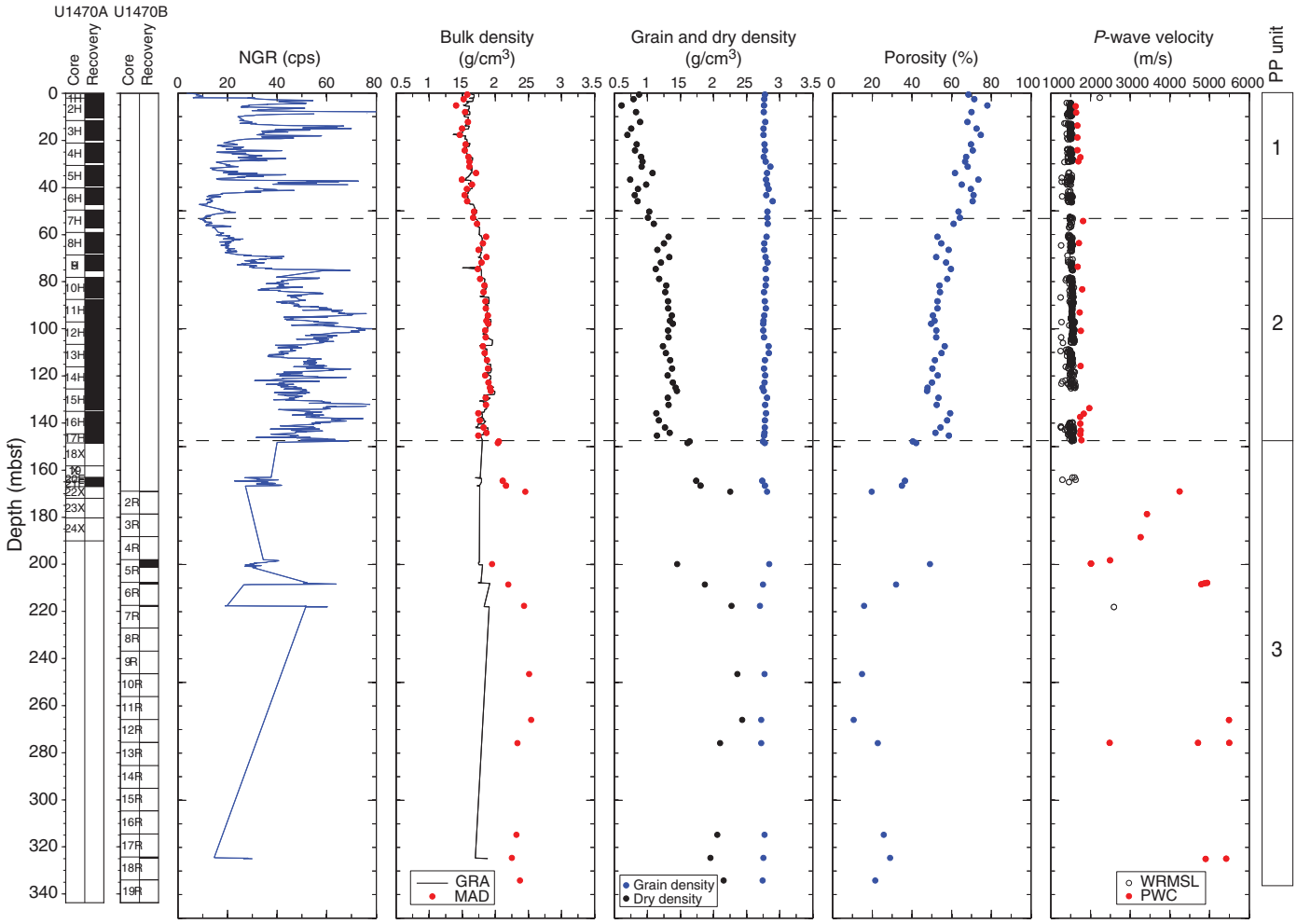

conductivity increases with decreasing water content and porosity (Figure **F27**).

Natural gamma radiation

NGR values in Unit 1 are characterized by several peaks with a large range between 10 and 80 counts/s (Figure **F26**). The top of Unit 2 starts with low NGR (10 counts/s) that increases to ~75 counts/s at 100 mbsf, In the lower part of Unit 2, NGR remains relatively high with several excursions. Unit 3 is made up of platform carbonates with low recovery (see **Lithostratigraphy**). As a result, NGR measurements are scarce and do not display any discernible trend.

Density and porosity

In the soft sediments of Units 1 and 2 (0–148 mbsf), gamma ray attenuation (GRA) and MAD bulk densities are similar in value with an increasing trend ranging from ~1.3 to 2.0 g/cm^3 (Figure **F26**). However, in the lithified platform carbonates below 148 mbsf (lithostratigraphic Unit III; see **Lithostratigraphy**), GRA bulk density is consistently lower than the bulk density from MAD samples and is not interpreted here. In petrophysical Unit 1, bulk and dry densities display an increasing trend downcore, whereas grain density remains almost constant. A distinct increase in bulk and dry density occurs at the Unit 1/2 boundary, and both continue to increase down to the base of Unit 2 (148 mbsf). Grain densities remain relatively constant. The Unit 2/3 boundary is marked by a distinct increase in density at 148 mbsf. Within Unit 3, MAD bulk density ranges from 1.8 to 2.6 g/cm^3. Grain density shows a modest decrease in Unit 3, whereas dry density increases from 1.5 to 2.5 g/cm^3 downhole.

Porosity generally displays an inverse trend to the density measurements. In the unlithified sediments of Unit 1, porosity decreases with depth from 80% to 60%. A sharper decrease marks the Unit 1/2 boundary, below which porosity decreases more gradually to the base Unit 2. A distinct decrease at 148 mbsf marks the Unit 2/3 boundary. Within Unit 3, variability in porosity increases, and below 200 mbsf, porosity fluctuates between 10% and 20%.

P-wave velocity

P-wave velocity on whole-round cores is almost constant at approximately 1500 m/s within the upper 148 mbsf; thus, all whole-round data are not interpreted here. Split-core PWC measurements have average velocities of 1735 m/s in Units 1 and 2 (drift sediments) with a slight increase at the Unit 1/2 boundary (Figure **F26**). In Unit 3 (platform carbonates), only discrete measurements could be performed on pieces and cylinder samples. In Unit 3, PWC mea-

Figure F27. Thermal conductivity, shear strength, and water content, Site U1470.

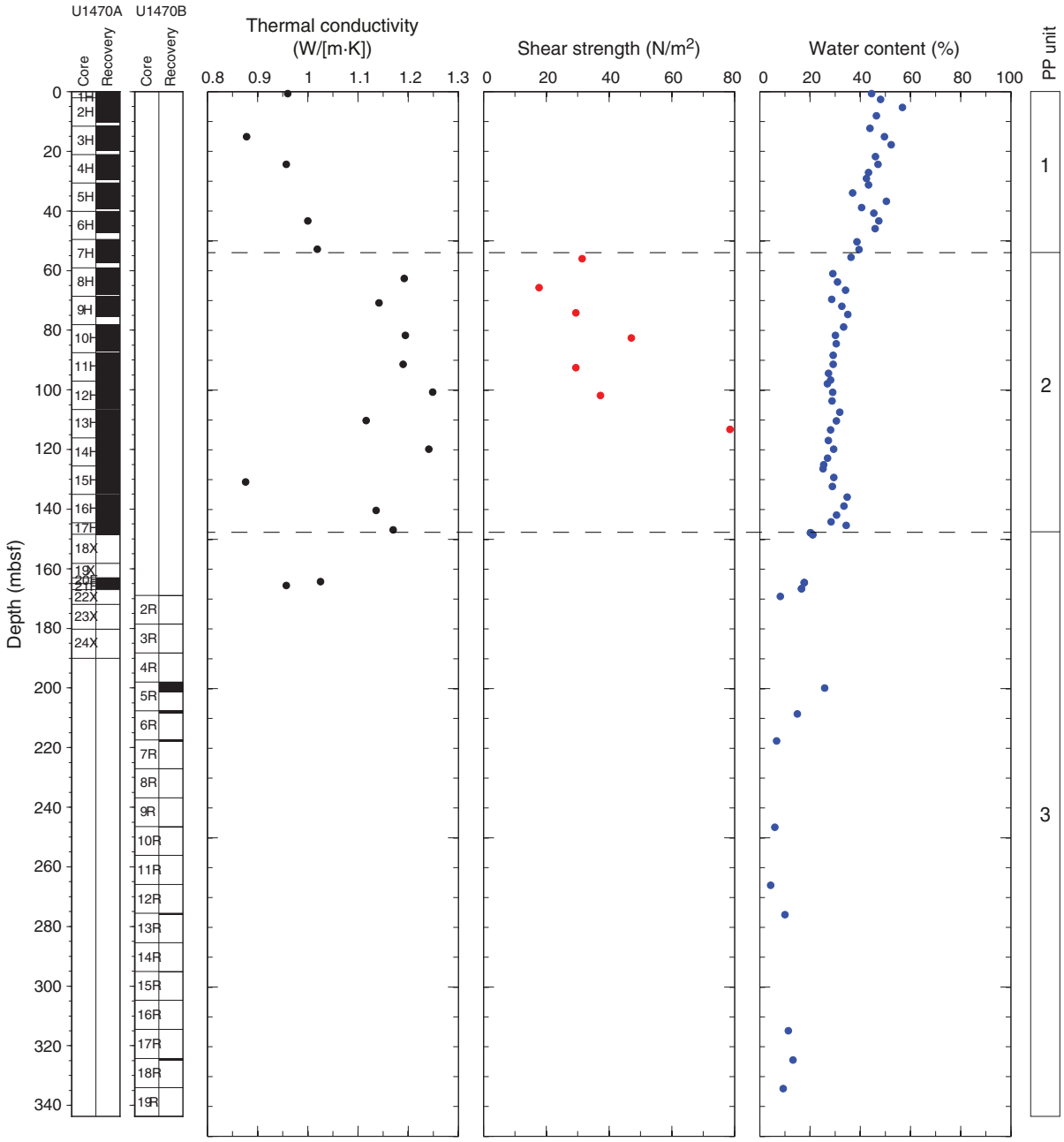

surements recorded high velocities from 2000 to more than 5000 m/s, which may be related to recrystallized dolomitic intervals below this depth.

Color reflectance

L* (total reflected light) is highly variable, resulting from dark-light color alternations in the upper parts of the cores (Figure **F25**). L* increases downhole in Unit 1 (0–54 mbsf). Higher L* reflectance likely corresponds to increased aragonite contents in the upper 100 mbsf (see **Geochemistry**). Below the Unit 1/2 boundary (54 mbsf), L* fluctuates about 50. Darker colors occur in zones of highest dolomitization, and colors are slightly lighter in cores with some preserved aragonite. a* values fluctuate from the seafloor to 150 mbsf ranging from 3 to 5 together with some spikes of >5. Below 148 mbsf, a* values remain relatively constant. Most b* values vary from 0 to 10 with an overall decrease with depth to 150 mbsf with highly variable values below 150 mbsf.

Magnetic susceptibility

Magnetic susceptibility loop (MSL or Whole-Round Multisensor Logger [WRMSL] MS) and magnetic susceptibility point (MSP or Section Half Multisensor Logger [SHMSL] MS) measurements show similar trends. MSP values are highly affected by coring contamination; hence, peaks above 3 IU were eliminated. MSP profiles range between 0 and –15 IU, showing a modest cycle in Units 1 and 2. Below 148 mbsf, MSP values are low (–10 and –5 IU) and too sparse to discern a trend (Figure **F25**). MSL profiles exhibit lower variability, between –3 and 3 IU.

Table T12. Thermal conductivity (TC), Site U1470. NA = not applicable. **Download table in .csv format**.

Core, section	Depth CFS-A (m)	TC measurement (W/[m·K])	TC mean (W/[m·K])	TC standard deviation (W/[m·K])	Rock type
359-U1470A-					
1H-1	0.700	0.960	0.960	NA	Soft
3H-3	15.050	0.880	0.878	0.002	Soft
3H-3	15.050	0.878			Soft
3H-3	15.050	0.877			Soft
4H-3	24.350	0.960	0.957	0.003	Soft
4H-3	24.350	0.955			Soft
4H-3	24.350	0.956			Soft
6H-3	43.300	1.003	1.000	0.003	Soft
6H-3	43.300	0.999			Soft
6H-3	43.300	0.997			Soft
7H-3	52.810	1.018	1.019	0.002	Soft
7H-3	52.810	1.022			Soft
7H-3	52.810	1.018			Soft
8H-3	62.560	1.191	1.192	0.001	Soft
8H-3	62.560	1.193			Soft
8H-3	62.560	1.193			Soft
9H-3	70.800	1.165	1.142	0.020	Soft
9H-3	70.800	1.129			Soft
9H-3	70.800	1.131			Soft
10H-3	81.610	1.210	1.194	0.014	Soft
10H-3	81.610	1.187			Soft
10H-3	81.610	1.185			Soft
11H-3	91.310	1.209	1.190	0.017	Soft
11H-3	91.310	1.178			Soft
11H-3	91.310	1.183			Soft
12H-3	100.660	1.245	1.249	0.004	Soft
12H-3	100.660	1.249			Soft
12H-3	100.660	1.253			Soft
13H-3	110.240	1.133	1.116	0.024	Soft
13H-3	110.240	1.099			Soft
14H-3	119.800	1.242	1.241	0.002	Soft
14H-3	119.800	1.239			Soft
14H-3	119.800	1.242			Soft
15H-4	130.800	0.871	0.876	0.010	Soft
15H-4	130.800	0.887			Soft
15H-4	130.800	0.869			Soft
16H-4	140.300	1.127	1.136	0.009	Soft
16H-4	140.300	1.136			Soft
16H-4	140.300	1.144			Soft
17H-2	146.800	1.170	1.170	0.003	Soft
17H-2	146.800	1.167			Soft
17H-2	146.800	1.172			Soft
20F-2	164.160	1.028	1.025	0.007	Soft
20F-2	164.160	1.031			Soft
20F-2	164.160	1.017			Soft
21F-1	165.500	0.957	0.957	NA	Soft

Thermal conductivity

Thermal conductivity was measured on whole-round sections with a full-space needle probe for soft sediments from Hole U1470A (Table **T12**; Figure **F27**). Thermal conductivity varies between ~0.85 and 1.25 W/(m·K) in Units 1 and 2 (0–148 mbsf) with a noted increase in Unit 2. The uppermost samples near the seafloor show values close to the thermal conductivity of seawater (0.6 W/[m·K]). These low values reflect the high water content in these coarse uncemented sediments. The downhole increase of thermal conductivity correlates with decrease of water saturation. In Unit 3, two carbonate platform samples have relatively low thermal conductivity values (0.9 and 1.0 W/[m·K] at ~164 mbsf).

Shear strength

Soft-sediment shear strength ranges from ~20 to 80 N/m^2 with the deepest measurement recording the highest value (Figure **F27**). Increasing shear strength with depth is similar to patterns observed at Sites U1466 and U1467. At all sites, the lack of a clear trend and the large scatter are likely due to limited test numbers and the variable composition of the drift sediments.

Downhole measurements

Logging operations and log data

Logging operations for Site U1470 began after completion of RCB coring in Hole U1470B to a total depth of 343.7 m drilling depth below seafloor (DSF) shortly after 0400 h (local time) on 17 November 2015. As a result of the challenging hole conditions during drilling (see **Operations**) and the potential for hole instability, a single logging run was planned with a tool string designed to measure the highest priority data. The sonic-resistivity tool string measuring gamma ray, sonic velocity, electrical resistivity, and borehole diameter was rigged up at 0730 h. Sea state was calm, with an average heave of 0.1 m peak-to-peak, so the wireline heave compensator was not used. The tool string was run into the hole, but unfortunately, resistance was encountered within 10 m below the base of the pipe at 103.5 m wireline log depth below seafloor (WSF). After multiple attempts to pass the blocked section of the borehole, during which the tool string reached ~52 m below the pipe, it was determined that no further logging should be attempted. The tool string was retrieved to the rig floor and rigged down, and logging operations were completed by 1215 h.

A limited set of logging data were recorded in Hole U1470B: gamma ray data extend from the pipe at 103.5 m to ~156 m WSF and resistivity data extend to only ~133 m WSF. Borehole diameter measurements were not possible because the caliper arm could not be opened in the collapsing borehole. Sonic measurements were not considered valid for the same reason. The available data were collected under highly unstable borehole conditions and, as such, are of uncertain quality. Logging data were not included in shipboard interpretation because of these limitations.

Logging data recorded in Hole U1470B are summarized in Figure **F28**. Recorded data were processed on shore as described in **Downhole measurements** in the Expedition 359 methods chapter (Betzler et al., 2017a). Detailed processing information can be found in standard data processing notes that accompany the logging data from Hole U1470B in the online IODP Log database (**http://iodp.ldeo.columbia.edu/DATA**).

Figure F28. Logs recorded during aborted logging run with sonic-resistivity tool string, Hole U1470B. Resistivity: R3 = medium resistivity, R5 = deepest resistivity, RT = true resistivity, modeled from all depths of investigation.

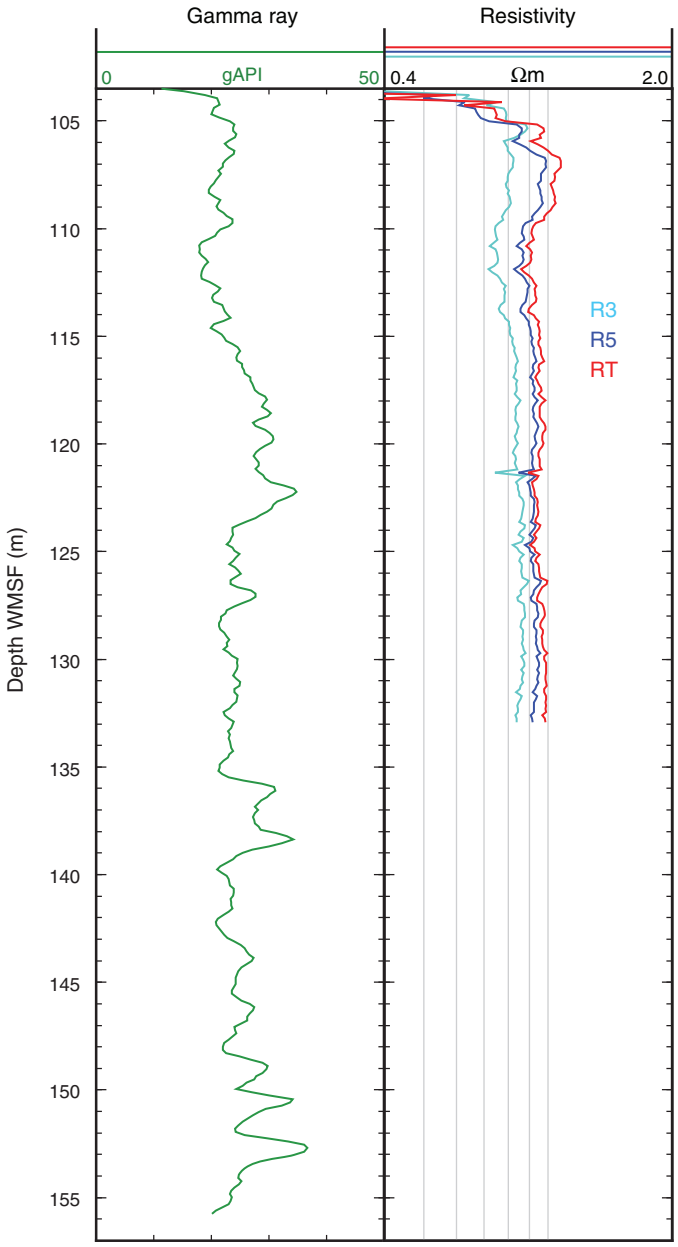

Seismic stratigraphy

Site U1470, the platform site of the southern transect, lies approximately 8 km south of the Goidhoo atoll in the southern branch of the Kardiva Channel (Figure **F1**). Tracing seismic reflections and sequence boundaries across the site survey data indicates that the platform at Site U1470 drowned at a later stage than in the northern branch of the Kardiva Channel and after deposition of DS2 (Figure **F29**).

Time-depth conversion

For the time-depth conversion, the sonic velocities of northern transect Site U1465, which has a very similar lithologic succession, were applied to the unlithified to partly lithified carbonate sands of the drifts (Figure **F30**). At both sites, a drift succession overlies a drowned carbonate platform. At the contact between these two packages is a strong contrast in acoustic impedance. For the drifts, a sonic velocity of 1.65 km/s was used as the interval velocity, and 2.6 km/s was used for the carbonate platform that is coeval to the first two drift sequences identified in the northern transect. Another increase in velocity to 3.5 km/s was observed in the transition to the carbonate platform deposits of platform sequence (PS) PS10 (Figure **F31**). This range is in line with drift sediment *P*-wave velocities measured on the SHMSL and compare well to the sonic velocity range measured on discrete core samples for the platform carbonates (see **Physical properties**).

Seismic facies and geometries

The drift sequences overlying the drowned platform show subparallel semicontinuous reflections, mainly of medium amplitude (Figures **F29**, **F31**; Table **T13**). The top of the drowned carbonate platform is indicated by a strong reflection of lower frequency. This drowning unconformity is at the top of DS2. Around 400 m to the west, this platform package thins out, and DS3 and DS2 almost merge. DS1 and DS2 at this location therefore represent a platform succession that postdates the drowning event recognized at Sites U1465 and U1469.

DS1 has internal layering that dips basinward to the east and becomes horizontal to the west. DS2 is characterized by an elevated top and shows basinward-dipping reflections in its eastern part. To the west, these reflections abut the basal sequence boundary of DS3, which can be explained by two processes. This stratal pattern could either show a late-stage predrowning reef package, or it may reflect erosion of the reef-related strata.

Core-seismic correlation

DS10 and DS9 correspond to lithostratigraphic Unit I, which consists of unlithified planktonic foraminifer-rich grainstone (see **Lithostratigraphy**). This package is followed by partly lithified bioclastic grain- to packstone in Unit II that covers the top of the platform and comprises DS3–DS8. The bounding unconformity of DS3 corresponds to the top of the shallow-water platform limestone (lithostratigraphic Unit III), which together with the overlying unconsolidated carbonate drift sands produces a reflection with a high acoustic impedance contrast. Downcore, the reefal limestone of the platform is interrupted with a thick layer of bioclastic grain- to rudstone (lithostratigraphic Unit IV) that corresponds to DS1. The top of the underlying coral-rich boundstone and floatstone is the reflector for Sequence Boundary DS1 (Figure **F31**).

No biostratigraphic ages could be extracted from the platform succession in DS1 and DS2. In the overlying drift strata, calcareous nannofossils and planktonic foraminifers document a Pleistocene age for the youngest two drift sequences (DS9 and DS10). DS8 is likely late Pliocene based on a nannofossil date. Below 80 mbsf to the top of the platform at 148.5 mbsf, microfossil preservation was poor, but a late Miocene planktonic foraminifer was found at around 120 mbsf (see **Biostratigraphy**).

Figure F29. Seismic section of the drowned carbonate platform that is onlapped and buried by drift sequences. Site U1470 is located at the edge of the drowned platform. Dark blue line marks horizon between platform and drift sequences in the northern transect (base of DS1). Site U1470 was cored at a location where drowning of the local carbonate bank postdates DS1 deposition.

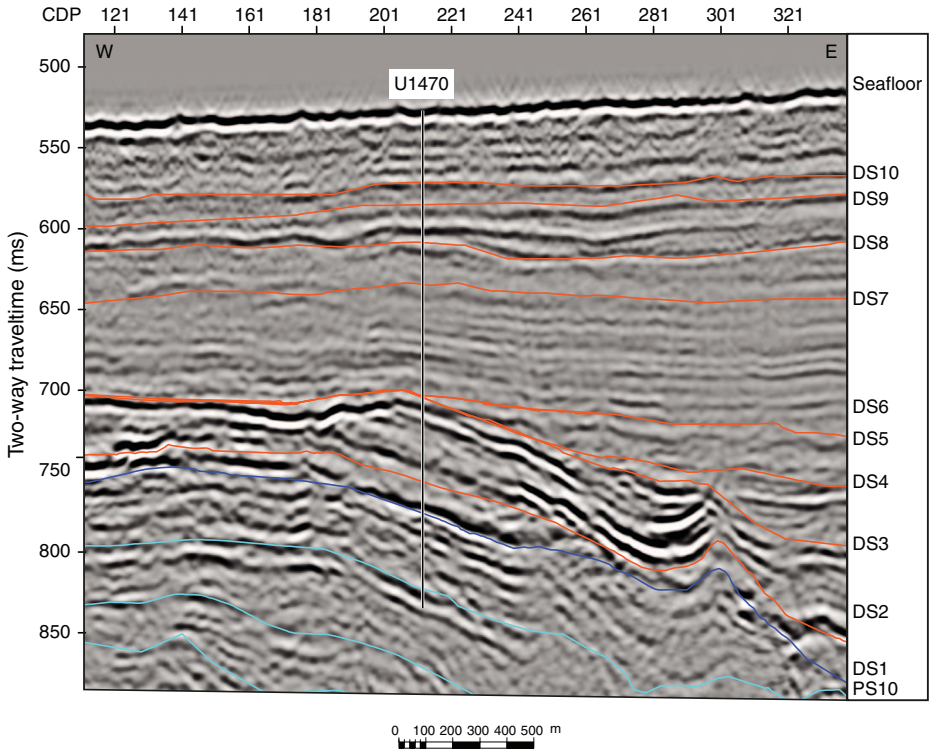

Figure F30. Time-depth conversion, Site U1470.

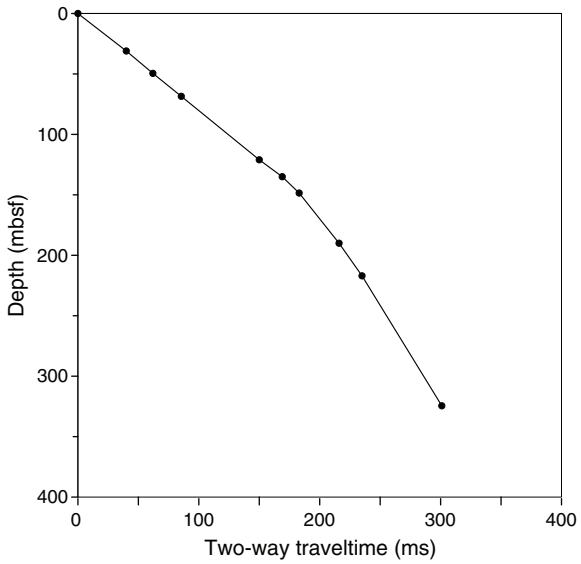

Figure F31. Correlation of seismic and core data, Site U1470. Seismic Line 32 (SO236) is shown with the platform and drift sequences. The interval velocity is used for the time-depth conversion.

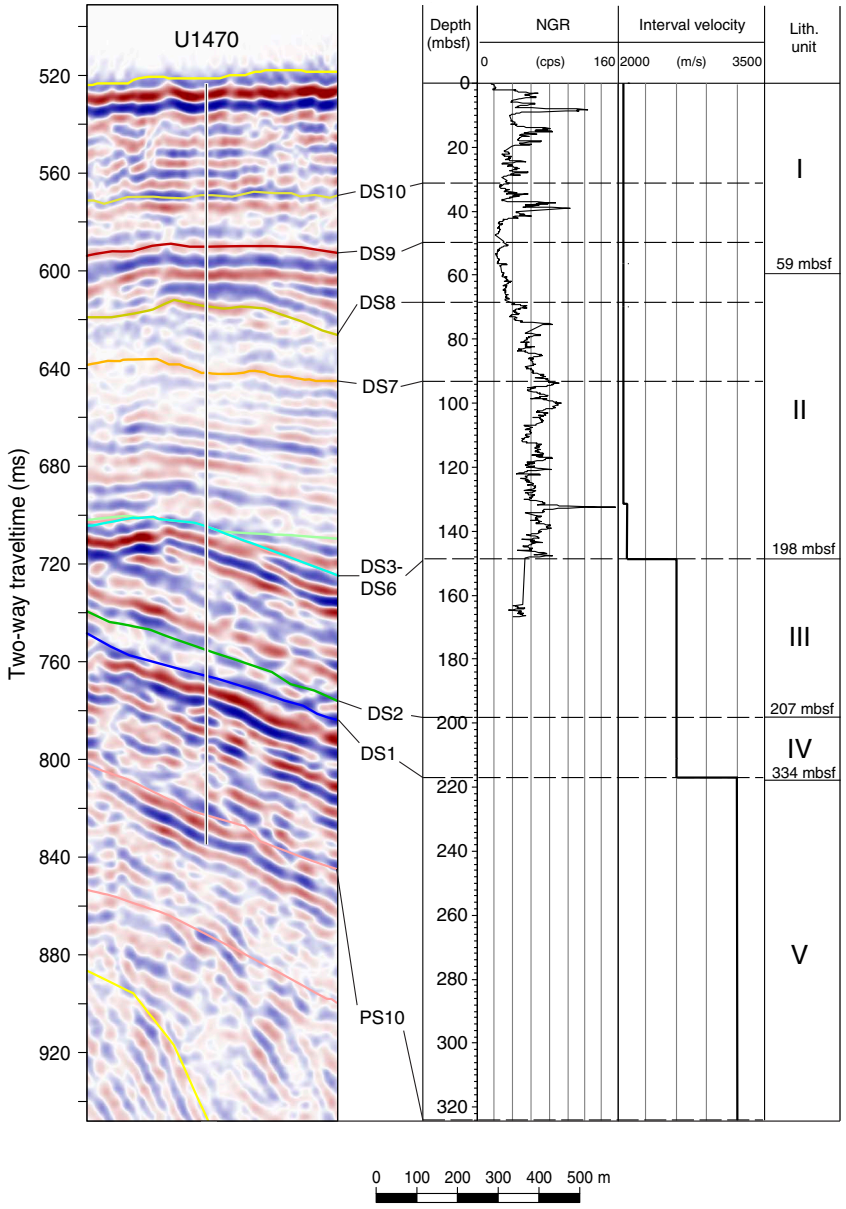

Table T13. Drift sequences and platform sequences, Site U1470. **Download table in .csv format.**

Sequence (bottom)	TWT (ms)	Depth (mbsf)
DS10	40	31
DS9	61	49
DS8	97.5	78
DS7	115	93
DS5–DS3	183	148.5
DS2	222	198
DS1	235	217
PS10	301	324.5

References

Belopolsky, A.V., and Droxler, A.W., 2004. Seismic expressions and interpretation of carbonate sequences: the Maldives platform, equatorial Indian Ocean. *AAPG Studies in Geology,* 49. **http://archives.datapages.com/data/specpubs/study49/images/st49.pdf**

Betzler, C., Eberli, G.P., Alvarez Zarikian, C.A., Alonso-García, M., Bialik, O.M., Blättler, C.L., Guo, J.A., Haffen, S., Horozal, S., Inoue, M., Jovane, L., Kroon, D., Lanci, L., Laya, J.C., Ling Hui Mee, A., Lüdmann, T., Nakakuni, M., Nath, B.N., Niino, K., Petruny, L.M., Pratiwi, S.D., Reijmer, J., Reolid, J., Slagle, A.L., Sloss, C.R., Su, X., Swart, P.K., Wright, J.D., Yao, Z., and Young, J.R., 2017a. Expedition 359 methods. *In* Betzler, C., Eberli, G.P., Alvarez Zarikian, C.A., and the Expedition 359 Scientists, *Maldives Monsoon and Sea Level.* Proceedings of the International Ocean Discovery

Program, 359: College Station, TX (International Ocean Discovery Program). **http://dx.doi.org/10.14379/iodp.proc.359.102.2017**

Betzler, C., Eberli, G.P., Alvarez Zarikian, C.A., Alonso-García, M., Bialik, O.M., Blättler, C.L., Guo, J.A., Haffen, S., Horozal, S., Inoue, M., Jovane, L., Kroon, D., Lanci, L., Laya, J.C., Ling Hui Mee, A., Lüdmann, T., Nakakuni, M., Nath, B.N., Niino, K., Petruny, L.M., Pratiwi, S.D., Reijmer, J., Reolid, J., Slagle, A.L., Sloss, C.R., Su, X., Swart, P.K., Wright, J.D., Yao, Z., and Young, J.R., 2017b. Expedition 359 summary. *In* Betzler, C., Eberli, G.P., Alvarez Zarikian, C.A., and the Expedition 359 Scientists, *Maldives Monsoon and Sea Level.* Proceedings of the International Ocean Discovery Program, 359: College Station, TX (International Ocean Discovery Program). **http://dx.doi.org/10.14379/iodp.proc.359.101.2017**

Betzler, C., Fürstenau, J., Lüdmann, T., Hübscher, C., Lindhorst, S., Paul, A., Reijmer, J.J.G., and Droxler, A.W., 2013a. Sea-level and ocean-current control on carbonate-platform growth, Maldives, Indian Ocean. *Basin Research*, 25(2):172–196. **http://dx.doi.org/10.1111/j.1365-2117.2012.00554.x**

Betzler, C., Hübscher, C., Lindhorst, S., Reijmer, J.J.G., Römer, M., Droxler, A.W., Fürstenau, J., and Lüdmann, T., 2009. Monsoon-induced partial carbonate platform drowning (Maldives, Indian Ocean). *Geology,* 37(10):867–870. **http://dx.doi.org/10.1130/G25702A.1**

Betzler, C., Lüdmann, T., Hübscher, C., and Fürstenau, J., 2013b. Current and sea-level signals in periplatform ooze (Neogene, Maldives, Indian Ocean). *Sedimentary Geology*, 290:126–137. **http://dx.doi.org/10.1016/j.sedgeo.2013.03.011**

Eberli, G.P., Anselmetti, F.S., Isern, A.R., and Delius, H., 2010. Timing of changes in sea-level and currents along Miocene platforms on the Marion Plateau, Australia. *In* Morgan, W.A., George, A.D., Harris, P.M., Kupecz, J.A., and Sarg, J.F. (Eds.), *Cenozoic Carbonate Systems of Australasia.* Special Publication - SEPM (Society for Sedimentary Geology), 95:219–242. **http://dx.doi.org/10.2110/sepmsp.095.219**

Ehrenberg, S.N., McArthur, J.M., and Thirlwall, M.F., 2006. Growth, demise, and dolomitization of Miocene carbonate platforms on the Marion Plateau, offshore NE Australia. *Journal of Sedimentary Research,* 76:91–116. **http://dx.doi.org/10.2110/jsr.2006.06**

Ginsburg, R.N., Lloyd, R.M., McCallum, J.S., Stockman, K.W., and Moody, R.A., 1958. *Surface Sediments of Great Bahama Bank:* Houston (Shell Development Company).

Gradstein, F.M., Ogg, J.G., Schmitz, M.D., and Ogg, G.M. (Eds.), 2012. *The Geological Time Scale 2012:* Amsterdam (Elsevier).

Hallock, P., 2005. Global change and modern coral reefs: new opportunities to understand shallow-water carbonate depositional processes. *Sedimentary Geology,* 175(1–4):19–33. **http://dx.doi.org/10.1016/j.sedgeo.2004.12.027**

Harris, P.M., Kendall, C.G.St.C., and Lerche, I., 1985. Carbonate cementation—a brief review. *In* Schneidermann, N., and Harris, P.M. (Eds.), *Carbonate Cements.* Special Publication - SEPM (Society for Sedimentary Geology), 36:79–95. **http://dx.doi.org/10.2110/pec.85.36.0079**

Hilgen, F.J., Lourens, L.J., and Van Dam, J.A., 2012. The Neogene period. With contributions by A.G. Beu, A.F. Boyes, R.A. Cooper, W. Krijgsman, J.G. Ogg, W.E. Piller, and D.S. Wilson. *In* Gradstein, F.M., Ogg, J.G., Schmitz, M.D., and Ogg, G.M. (Eds.), *The Geologic Time Scale:* Oxford, United Kingdom (Elsevier), 923–978. **http://dx.doi.org/10.1016/B978-0-444-59425-9.00029-9**

Lourens, L., Hilgen, F., Shackleton, N.J., Laskar, J., and Wilson, D., 2004. The Neogene period. *In* Gradstein, F.M., Ogg, J.G., and Smith, A. (Eds.), *A Geologic Time Scale 2004:* Cambridge, United Kingdom (Cambridge University Press), 409–440. **http://dx.doi.org/10.1017/CBO9780511536045.022**

Lüdmann, T., Kalvelage, C., Betzler, C., Fürstenau, J., and Hübscher, C., 2013. The Maldives, a giant isolated carbonate platform dominated by bottom currents. *Marine and Petroleum Geology*, 43:326–340. **http://dx.doi.org/10.1016/j.marpetgeo.2013.01.004**

Raffi, I., Backman, J., Fornaciari, E., Pälike, H., Rio, D., Lourens, L., and Hilgen, F., 2006. A review of calcareous nannofossil astrobiochronology encompassing the past 25 million years. *Quaternary Science Reviews,* 25(23–24):3113–3137. **http://dx.doi.org/10.1016/j.quascirev.2006.07.007**

Riegl, B.M., Halifar, J., Purkis, S.J., and Godinez-Orta, L., 2007. Sedimentary facies of the eastern Pacific's northernmost reef-like setting (Cabo Pulmo, Mexico). *Marine Geology,* 236(1–2):61–77. **http://dx.doi.org/10.1016/j.margeo.2006.09.021**

Swart, P.K., 2000. The oxygen isotopic composition of interstitial waters: evidence for fluid flow and recrystallization in the margin of the Great Bahama Bank. *In* Swart, P.K., Eberli, G.P., Malone, M.J., and Sarg, J.F. (Eds.), *Proceedings of the Ocean Drilling Program, Scientific Results,* 166: College Station, TX (Ocean Drilling Program), 91–98. **http://dx.doi.org/10.2973/odp.proc.sr.166.130.2000**

Thompson, P.R., Bé, A.W.H., Duplessy, J.-C., and Shackleton, N.J., 1979. Disappearance of pink-pigmented *Globigerinoides ruber* at 120,000 yr BP in the Indian and Pacific Oceans. *Nature,* 280(5723):554–558. **http://dx.doi.org/10.1038/280554a0**

Wade, B.S., Pearson, P.N., Berggren, W.A., and Pälike, H., 2011. Review and revision of Cenozoic tropical planktonic foraminiferal biostratigraphy and calibration to the geomagnetic polarity and astronomical time scale. *Earth-Science Reviews,* 104(1–3):111–142. **http://dx.doi.org/10.1016/j.earscirev.2010.09.003**

Warne, M.T., 1988. *Neonesidea* and *Bairdoppilata* (Ostracoda) from the Miocene of the Port Phillip and Western Port Basins, Victoria, Australia. *Alcheringa: An Australasian Journal of Palaeontology,* 12(1):7–26. **http://dx.doi.org/10.1080/03115518808618993**

Zhao, Q., Whatley, R., and Zhou, B., 2000. The taxonomy and distribution of recent species of the ostracod genus *Cytheropteron* in the South China Sea. *Revista Espanola de Micropaleontologia,* 32(2):259–281.